Pergamon

Geochimica et Cosmochimica Acta, Vol. 67, No. 10, pp. 1821–1836, 2003
Copyright © 2003 Elsevier Science Ltd
Printed in the USA. All rights reserved
0016-7037/03 $30.00 + .00

doi:10.1016/S0016-7037(00)01281-4

Thermodynamic properties of the Sb(III) hydroxide complex $Sb(OH)_{3(aq)}$ at hydrothermal conditions

A. V. Zotov,[1] N. D. Shikina,[1,*] and N. N. Akinfiev[2]

[1]Institute of Geology of Ore Deposits, Petrography, Mineralogy and Geochemistry RAS, Staromonetnyi per. 35, Moscow 119017, Russia
[2]Department of Chemistry, Moscow State Geological Prospecting Academy, Miklukho-Maklai str. 23, Moscow 117873, Russia

(*Received June* 8, 2001; *accepted in revised form August* 27, 2002)

Abstract—The standard thermodynamic properties and Helgeson-Kirkham-Flowers (HKF) parameters for $Sb(OH)_{3(aq)}$ have been estimated. For this purpose, the available solubility data for senarmontite, valentinite, stibnite, and native Sb in a wide range of temperatures (15 to 450°C) and pressures (1 to 1000 bar), and thermodynamic properties of Sb oxides (senarmontite and valentinite) have been critically analyzed. Published data were complimented by results from new experiments performed by solubility and solid-state galvanic cell methods. Both experimental data and thermodynamic calculations show that the hydroxide complex $Sb(OH)_{3(aq)}$ is primarily responsible for hydrothermal transport of antimony, especially at temperatures above 250°C. *Copyright © 2003 Elsevier Science Ltd*

1. INTRODUCTION

Antimony (Sb) is an important component of hydrothermal systems, as demonstrated by the fact that many epithermal ore deposits contain high concentrations of this element. Antimony is commonly present in sulfide ores as stibnite (Sb_2S_3) or various sulfosalts, and in some cases as native Sb (Williams-Jones and Normand, 1997). Natural geothermal systems generally contain appreciable concentrations of antimony, typically on the order of some parts per million (White, 1967; Stauffer and Thompson, 1984; Alekhin et al., 1987; Karpov, 1988; Krupp and Seward, 1990).

Antimony is present in two oxidation states in crustal fluids, Sb(III) and Sb(V). Under surface oxidizing conditions, Sb(V) may be predominant (Pourbaix, 1966; Krainov et al., 1979), whereas Sb-bearing hydrothermal fluids mainly contain Sb(III) (Spycher and Reed, 1989; Shikina and Zotov, 1990). However, in the recent extended X-ray absorption fine structure study, Mosselmans et al. (2000) proposed the formation of Sb(V) species at high temperatures (up to 200°C) in alkaline sulfide solutions. On the other hand, X-ray absorption fine structure (XAFS) spectroscopic measurements of Pokrovski G., Roux J., Testemale D., and Hazemann J–L. (unpublished data) did not detect any traces of Sb (V) in H_2O in equilibrium with Sb_2O_3 at temperatures from 200 to 450°C. The present study deals with experimental data for Sb(III) aqueous species.

The main Sb(III) species in natural hydrothermal solutions are considered to be hydroxide and sulfide complexes (Sorokin et al., 1988; Spycher and Reed, 1989). Only in strongly acid solutions is antimony speciation believed to be dominated by chloride complexes (Wood et al., 1987; Belevantsev et al., 1998a; Oelkers et al., 1998). Sulfide complexes have been studied at low temperature by Akeret (1953), Babko and Lisetskaya (1956), Arnston et al. (1966), and Kolpakova (1971). They were also studied by Learned et al. (1974), Kolpakova (1982a), Nekrasov and Konyushok (1982), Krupp (1988), Wood (1989), Belevantsev et al. (1998b), Gushchina et al. (2000), and Mosselmans et al. (2000) over a wide temperature range (up to 350°C). However, as shown by Popova et al. (1975), Spycher and Reed (1989), Sorokin et al. (1988), and Zotov et al. (1995), at temperatures greater than 200 to 250°C, the hydroxide species predominate in slightly acid and neutral solutions even in sulfide-bearing systems. According to these studies, $Sb(OH)_{3(aq)}$ is predominant over a wide range of pH and appears to be mainly responsible for the hydrothermal transport of antimony, especially at temperatures above 200°C.

The goal of the present study was to provide reliable thermodynamic properties for the $Sb(OH)_{3,(aq)}$ species to describe antimony behavior over a wide range of temperature and pressure. Estimates of these properties have been published previously by Sorokin et al. (1988) for temperatures up to 300°C under saturated vapor pressure and by Akinfiev et al. (1993) for temperatures and pressures up to 500°C and 2 kbar, respectively. However, subsequent experimental studies of Sb_2O_3 and Sb_2S_3 solubility (Shikina and Zotov, 1996, 1999) indicate a need to refine these data. In this article, we report the results of a critical analysis of available experimental data on the solubility of senarmontite, valentinite, stibnite, and native Sb, and the thermodynamic properties of Sb-oxides (senarmontite and valentinite). To verify and refine some questionable points, we also conducted some additional experiments. As a result, an internally consistent set of standard thermodynamic properties and Helgeson-Kirkham-Flowers (HKF) equation-of-state parameters for $Sb(OH)_{3(aq)}$ within the framework of the revised HKF (Tanger and Helgeson, 1988) model have been derived.

2. SOLUBILITY OF THE SB-BEARING SOLID PHASES

2.1. Solubility of Valentinite (Sb_2O_3, rhom) and Senarmontite (Sb_2O_3, cub)

The solubility of Sb_2O_3 in aqueous solutions is independent of pH (1.5 to 12) at 25°C (Gayer and Garrett, 1952; Vasil'ev and Shorokhova, 1972b, 1973). This indicates that Sb_2O_3 dissolves by forming the neutral species $Sb(OH)_{3(aq)}$ according to the reactions

* Author to whom correspondence should be addressed (azotov@igem.ru).

Table 1. Valentinite solubility in H_2O and log $K^0_{(1)}$ at 1 bar.

T (°C)	$m_{sb} \times 10^4$ (mol·(kg H_2O)$^{-1}$)	log $K^0_{(1)}$	Reference
15	0.55	−4.26	Schulze, (1883)[a]
25	0.52 ± 0.1	−4.28 ± 0.08	Gayer and Garrett (1952)
80	2.02 ± 0.3[b]	−3.69 ± 0.06	This study (Appendix 1)
100	3.4	−3.47	Schulze (1883)[a]

[a] Cited in Gayer and Garrett (1952).
[b] In this and other tables the calculated uncertainty represents the confidence level 0.95.

$$0.5\ Sb_2O_{3(valentinite)} + 1.5\ H_2O = Sb(OH)_{3(aq)};\ K^\circ_{(1)} = a_{Sb(OH)_{3(aq)}} \quad (1)$$

$$0.5\ Sb_2O_{3(senarmontite)} + 1.5\ H_2O = Sb(OH)_{3(aq)};\ K^\circ_{(2)} = a_{Sb(OH)_{3(aq)}}. \quad (2)$$

Increasing temperature up to 350°C does not change Sb speciation in solution, and $Sb(OH)_{3(aq)}$ remains the dominant complex over a wide pH range (Shikina and Zotov, 1999). The stoichiometry of this species is supported by the recent XAFS spectroscopic study of Pokrovski G., Roux J., Testemale D., and Hazemann J–L. Their results indicate that in the temperature range 300 to 450°C, aqueous antimony in equilibrium with senarmontite has an oxidation state of +3 and is surrounded by 3 ± 0.5 oxygen atoms, in agreement with the $Sb(OH)_3$ stoichiometry.

The solubility of valentinite in H_2O was studied by Schulze (1883) and Gayer and Garrett (1952) at temperatures from 15 to 100°C. Solubility data and calculated values for the equilibrium constant of the corresponding dissolution reaction 1 are reported in Table 1. Figure 1 shows that log $K^\circ_{(1)}$ increases strongly with temperature. Our control experiment at 80°C (Appendix 1) is in good agreement with the available experimental data (Fig. 1).

Table 2. Senarmontite solubility in H_2O and corresponding values of log $K^0_{(2)}$.

T (°C)	P (bars)	$m_{Sb} \times 10^4$ (mol·(kg H_2O)$^{-1}$)	log $K^0_{(2)}$	Reference
80	1	1.1 ± 0.2	−3.96 ± 0.08	This study (Appendix 1)
90	1	3.1 ± 0.9	−3.51 ± 0.13	Popova et al. (1975)
200	P_{sat}	44.3 ± 5.0	−2.35 ± 0.05	
210	P_{sat}	52.2 ± 3.9	−2.28 ± 0.03	Shikina and Zotov (1990)
210	500	54.6 ± 5.1	−2.26 ± 0.04	
210	1000	58.0 ± 5.0	−2.24 ± 0.04	
300	P_{sat}	352 ± 2.8	−1.45 ± 0.04	
300	500	375 ± 1.4	−1.43 ± 0.02	
300	1000	384 ± 0.8	−1.42 ± 0.01	
350	P_{sat}	701 ± 60	−1.15 ± 0.04	This study (Appendix 2)
400	500	720 ± 50	−1.14 ± 0.03	This study (Appendix 5)

[a] P_{sat} = saturated vapor pressure.

The solubility of senarmontite in pure H_2O and slightly acidic solutions was measured by Popova et al. (1975) and Shikina and Zotov (1990) over a wide range of temperature (80 to 400°C) and pressure (1 to 1000 bars). These data are presented in Table 2. Senarmontite solubility increases slightly with pressure (Fig. 2) and sharply with temperature (Fig. 3). Our new experiments performed at 80 and 350°C (Appendices 1 and 2) confirm the linear dependence of log$K^\circ_{(2)}$ on reciprocal temperature at saturated vapor pressure (P_{sat}):

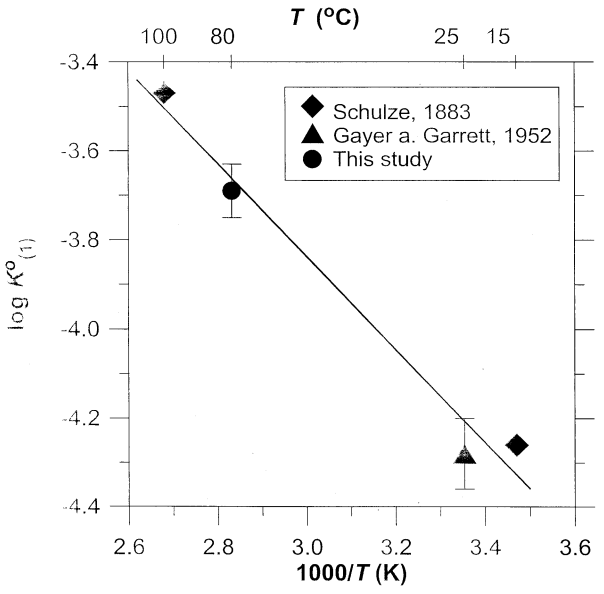

Fig. 1. Solubility of valentinite ($Sb_2O_{3(romb.)}$) expressed as log $K^\circ_{(1)}$ vs. reciprocal temperature. The symbols represent experimental data (Table 1) and the line shows a linear regression of these values.

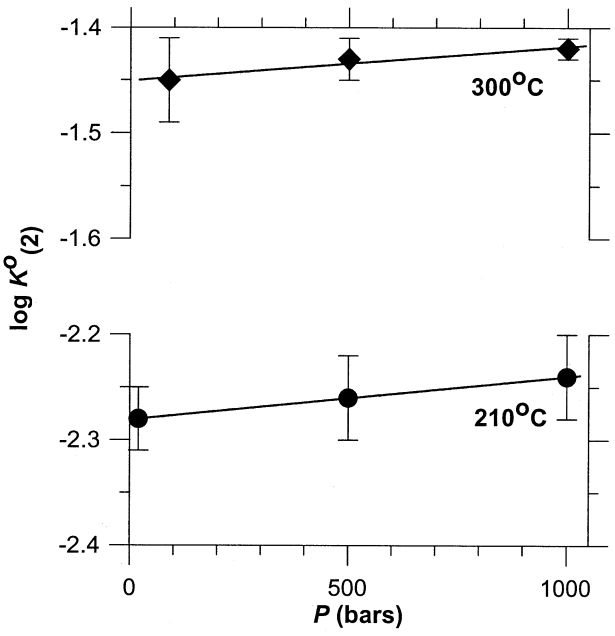

Fig. 2. Pressure dependence of log $K^\circ_{(2)}$ at 210°C and 300°C. The symbols denote experimental data (Table 2) and the lines represent linear regressions of these values.

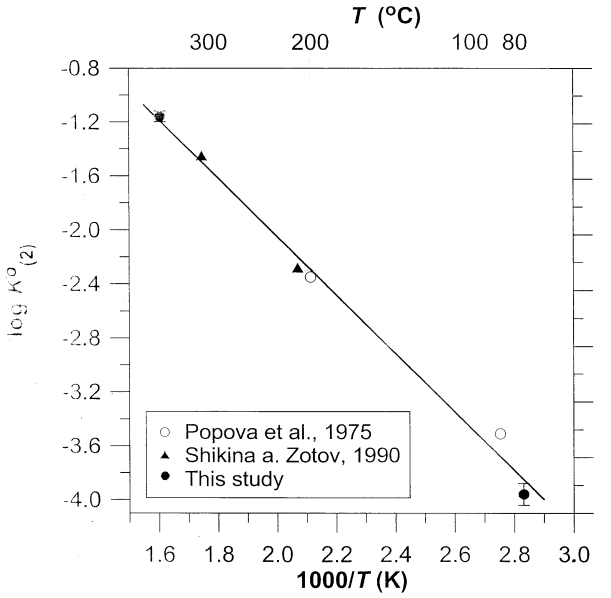

Fig. 3. Solubility of senarmontite ($Sb_2O_{3(cub.)}$) expressed as log $K°_{(2)}$ vs. reciprocal temperature at saturated vapor pressure. Symbols represent experimental data (Table 2), and the line represents a linear regression of the experimental values.

$$\log K°_{(2)} = -2165.7/T + 2.28. \quad (3)$$

2.2. Solubility of Metallic Antimony (Sb, trig)

The solubility of $Sb_{(metal)}$ was measured by Shikina and Zotov (1990) in water as a function of hydrogen fugacity at 450°C and 500 and 1000 bars. It was found that Sb solubility decreases linearly with increasing hydrogen fugacity (f_{H_2}), with slopes (log m_{Sb} vs log f_{H_2}) of -1.50 ± 0.35 and -1.37 ± 0.35 at 500 and 1000 bars, respectively (Fig. 4). This is consistent with the formation of $Sb(OH)_{3(aq)}$ according to the reaction

$$Sb_{(metal)} + 3H_2O = Sb(OH)_{3(aq)} + 1.5H_{2(g)}; \quad K°_{(4)} = a_{Sb(OH)_{3(aq)}} \times f_{H_2}^{1.5} \quad (4)$$

The average values of the equilibrium constant of reaction 4 cited from Shikina and Zotov (1990) are listed in Table 3.

2.3. Solubility of Stibnite (Sb_2S_3, rhom)

A number of experimental studies have been performed on the solubility of stibnite in pure water and slightly acidic solutions ($3<pH<7$) containing up to 0.01*m* H_2S at 200 to 350°C at P_{sat} and 500 bars and show that $Sb(OH)_{3(aq)}$ is predominant at these conditions (Kozlov, 1982; Wood et al., 1987; Akinfiev et al., 1993; Shikina and Zotov, 1996, 1999). Krupp (1988) studied Sb_2S_3 solubility in H_2S-rich solutions ($m_{H_2S} > 0.01m$) over a wide range of temperature, pH, and H_2S contents and attributed Sb_2S_3 dissolution to the formation of thioantimonite ($H_nSb_2S_{6-n}$, $0 < n < 2$) and hydroxo-thioantimonite ($Sb_2S_2(OH)_{2(aq)}$) complexes. However, we propose that at least at the highest temperature of Krupp's (1988) study (350°C), $Sb(OH)_{3(aq)}$ was also present in the acidic and neutral

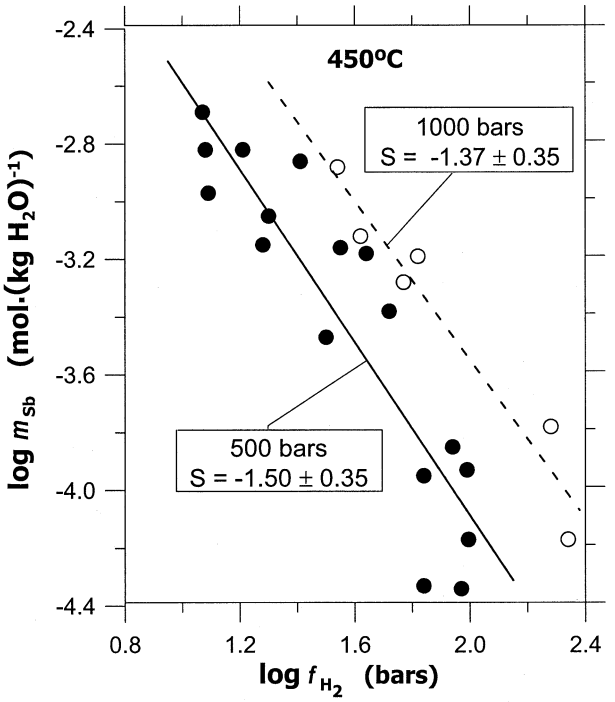

Fig. 4. $Sb_{(metal)}$ solubility at 450°C as a function of H_2 fugacity. Symbols represent experimental data for 500 and 1000 bars from Shikina and Zotov (1990). The lines represent a linear regression of the experimental values.

experimental solutions. Figure 5 shows that there is a linear relationship between stibnite solubility (log m_{Sb}) and sulfide concentration (log $m_{H_2S_{(aq)}}$) at 350°C. The experimental data points obtained at saturated vapor pressure (Krupp, 1988; Akinfiev et al., 1993) and 500 bars (Shikina and Zotov, 1996) shown in this figure exhibit the same relationship, demonstrating the weak influence of pressure on stibnite solubility. The slope of log m_{Sb} vs. log $m_{H_2S_{(aq)}}$ is -1.39 ± 0.12 (Fig. 5). This value is close to the theoretical slope (-1.5) for $Sb(OH)_{3(aq)}$ formation according to the reaction

$$0.5\ Sb_2S_{3(stibnite)} + 3\ H_2O = Sb(OH)_{3(aq)} + 1.5\ H_2S_{(aq)}; \quad K°_{(5)} = a_{Sb(OH)_{3(aq)}} \times a_{H_2S_{(aq)}}^{1.5} \quad (5)$$

A similar relationship can be seen in Figure 6, which shows experimental data on Sb_2S_3 solubility at 300 and 306°C (Shikina and Zotov, 1999). The logarithm of m_{Sb} exhibits a linear dependence on log $m_{H_2S_{(aq)}}$ with slopes -1.41 ± 0.07 and -1.30 ± 0.08 at 300 and 306°C, respectively, over a wide range of H_2S concentrations ($0.003 < m_{H_2S} < 0.1$). These values are close to the theoretical slope of -1.5 according to

Table 3. Equilibrium constants for reaction 4 at 450°C (Shikina and Zotov, 1990).

P (bars)	log $K°_{(4)}$
500	-1.09 ± 0.12
1000	-0.56 ± 0.14

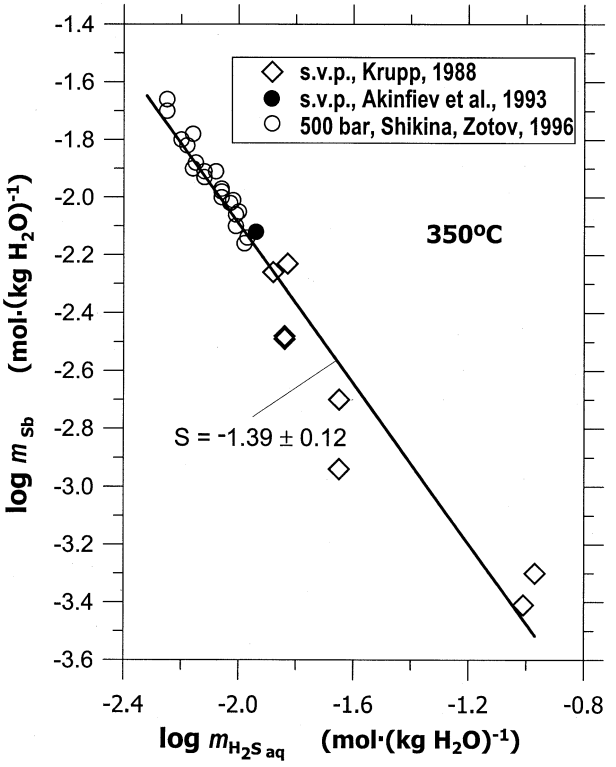

Fig. 5. Solubility of stibnite Sb_2S_3 vs. $H_2S_{(aq)}$ molality at 350°C at P_{sat} and 500 bar. The data from Krupp (1988) for H_2S concentration have been recalculated by reaction 5. Symbols represent experimental data and the line represents a linear regression of these values.

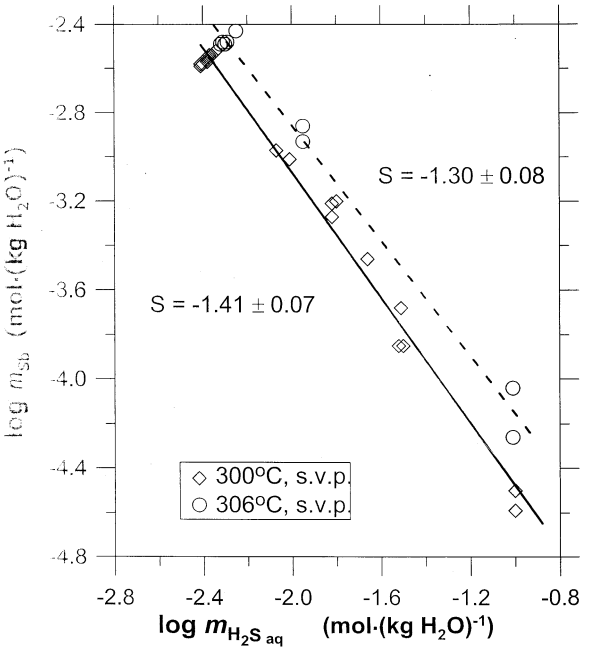

Fig. 6. The solubility of stibnite (Sb_2S_3) vs. $H_2S_{(aq)}$ molality at 300°C and 306°C under saturated vapor pressure. Data from Shikina and Zotov (1999). Symbols denote experimental data, and the lines represent a linear regression of the experimental values.

reaction 5. Thus, these results demonstrate that $Sb(OH)_{3(aq)}$ is the predominant Sb species at high temperature (300 to 350°C) in solutions with Sb and H_2S molalities up at least to 0.02 and 0.1, respectively (Shikina and Zotov, 1999). Thus, there is no need to assume formation of any dimeric aqueous species such as $Sb_2(OH)_6$ (Akinfiev et al., 1993) at these conditions.

Experimental data on stibnite solubility at temperatures from 198 to 350°C and the corresponding calculated values of the equilibrium constant for reaction 5 are presented in Table 4. Values of $\log K^\circ_{(5)}$ calculated from our measurements and available solubility data (Kozlov, 1982; Wood et al., 1987; Krupp, 1988) at P_{sat} are compared in Figure 7.

3. THERMODYNAMIC PROPERTIES OF THE ANTIMONY SOLID PHASES

The generation of thermodynamic properties of aqueous Sb species from solubility data requires corresponding properties for the solid Sb phases (valentinite $Sb_2O_{3(rhomb.)}$, senarmontite $Sb_2O_{3(cub.)}$, and stibnite Sb_2S_3).

3.1. Valentinite (Sb_2O_3, rhom)

The low-temperature heat capacity of valentinite was measured by Anderson (1930) and Gorgoraki and Tarasov (1965). It was noticed (Behrens and Rosenblatt, 1973; Popova et al., 1975) that the C_p values of Gorgoraki and Tarasov (1965) are higher by 4 to 5% than those of Anderson (1930). Behrens and Rosenblatt (1973) and Popova et al. (1975) explained this difference as due to systematic error in the measurements of Gorgoraki and Tarasov (1965). This systematic error for Sb_2O_3 is proved by the presence of the same difference (4 to 5%) between C_p values for another solid, $As_2O_{3(monoclinic)}$, reported by Gorgoraki and Tarasov (1965) and those measured later by Chang and Bestul (1971). For this reason, we have preferred to use the molal heat capacity and entropy of valentinite from Anderson's data, recalculated by Behrens and Rosenblatt (1973):

$$C^\circ_{p,\,298.15} = 24.29\ \text{cal·mol}^{-1}\text{·K}^{-1},$$

$$S^\circ_{298.15} = 29.43\ \text{cal·mol}^{-1}\text{·K}^{-1}.$$

These values are practically identical to those listed in the handbooks of Wagman et al. (1982) and Pankratz (1982) and similar to those presented by the IVTANTERMO database (Iorish et al., 1998). However, they differ markedly from those given by Glushko (1968) because the latter values were based on the measurements of Gorgoraki and Tarasov (1965).

The heat capacity of valentinite has not been measured above 300 K. We therefore estimated the high-temperature heat capacities of valentinite with the low-temperature heat capacities data of Anderson (1930) and the 3*Rn* computer code (Gurevich et al., 1997). The heat capacity measurements of Anderson (1930), recalculated by Behrens and Rosenblatt (1973) for the temperature range 250 to 300 K were extrapolated to higher temperature by the equation

$$C_p^\circ = 3Rn(1 - AT^{-1} + BT^{-2}) + CT, \qquad (6)$$

where R is the ideal gas constant, T is temperature (K), $n = 5$

Table 4. Stibnite solubility in water and slightly acidic aqueous solutions and log $K^0_{(5)}$.

T (°C)	P (bars)	Solution	$m_{Sb} \times 10^4$ (mol·(kg H_2O)$^{-1}$)	log $K^0_{(5)}$	Reference
198	500	H_2O	1.97	−9.00 ± 0.05	Shikina and Zotov (1999)
205	P_{sat}	H_2O	2.4	−8.79	
275	500	H_2O	14.4	−6.84 ± 0.05	
300	P_{sat}	H_2O	28	−6.12 ± 0.03	
300	P_{sat}	0.001*m* HCl + $H_2S_{(aq)}$		−6.04 ± 0.07	
306	P_{sat}	H_2O and 0.001*m* HCl	33	−5.93 ± 0.05	
306	P_{sat}	0.001*m* HCl + $H_2S_{(aq)}$		−5.80 ± 0.18	
350	P_{sat}	H_2O	76	−5.03 ± 0.10	Akinfiev et al. (1993)
350	500	H_2O	70	−5.12 ± 0.05	Shikina and Zotov (1996)
350	500	H_2O + $Sb_{(aq)}$		−5.06 ± 0.02	
350	P_{sat}	HCl + $H_2S_{(aq)}$		−5.12 ± 0.2	Krupp (1988)[a]
263	P_{sat}	H_2O	19	−6.54	Kozlov (1982)[b]
283	P_{sat}	H_2O	27	−6.16	
305	P_{sat}	H_2O	40	−5.74	
325	P_{sat}	H_2O	54	−5.41	
369	P_{sat}	H_2O	110	−4.69	
200	P_{sat}			−8.95 ± 0.2	Wood et al. (1987)[c]
250	P_{sat}			−7.80 ± 0.35	
300	P_{sat}			−6.25 ± 0.3	
350	P_{sat}			−5.55 ± 0.45	

[a] Solubility was recalculated using reaction 5.
[b] log $K^0_{(5)}$ was calculated in this study from the solubility data without considering the distribution of H_2S between liquid and vapor phases.
[c] Solubility data were measured for the FeS_2-FeS-F_3O_4-ZnS-PbS-Sb_2S_3-Bi_2S_3-Ag_2S-MoS_2-H_2O system.

(number of atoms in Sb_2O_3), and A, B, and C are empirical coefficients determined by least squares regression. The extrapolated C°_p values for the temperature interval from 290 K to the melting point of stibnite (928 K) were then fitted by the Maier-Kelley equation for consistency with available databases:

$$C^\circ_{p,\,Sb_2O_3,\,valentinite}\ (cal{\cdot}mol^{-1}{\cdot}K^{-1}) = 24.841 + 10.2 \times 10^{-3} \cdot T - 3.197 \times 10^5 \times T^{-2}. \quad (7)$$

According to this equation, the molal heat capacity of valentinite at the melting point (928 K) and its mean value for the temperature interval from 300 to 500 K is 33.8 and 26.7 cal·mol^{-1}·K^{-1}, respectively. These values are in good agreement both with the estimate of Behrens and Rosenblatt (1973) ($C^\circ_{p,928}$ = 35 cal · mol^{-1}·K^{-1}) and with the experimental measurement of mean molal heat capacity by Knauth and Schwitzgebel (1988) by the DSC Ar-method ($C^\circ_{p,300-500\ K}$ = 26.58 ± 0.28 cal·mol^{-1}·K^{-1}). By contrast, a 3*Rn*-code extrapolation of the low-temperature $C^\circ_{p\ (valentinite)}$ data of Gorgoraki and Tarasov (1965) yields values of 44.4 and 30.5 cal·mol^{-1}·K^{-1}, respectively. These values differ substantially from those of Behrens and Rosenblatt (1973) and Knauth and Schwitzgebel (1988). This provides further reason to prefer the low-temperature heat capacity data of Anderson (1930). Thus, Anderson's data recalculated by Behrens and Rosenblatt (1973) together with empirical Eqn. 7 were adopted in this study.

Values of the standard molar Gibbs formation energy of valentinite have been determined from experiments employing several methods.

1. Vasil'ev and Shorokhova (1972a), by use of a potentiometric method at 15 to 50°C, obtained a value for $\Delta_f G^\circ_{298,Sb_2O_3(valentinite)}$ of −149.30 ± 0.075 kcal·mol^{-1}. This value is close to that of Schuhmann (1924) (−149.0 kcal·mol^{-1}) but differs markedly from that of Roberts and Fenwick (1928) (−148.269 kcal·mol^{-1}). Schuhmann (1924) and Roberts and Fenwick (1928) also used potentiometric methods.

2. Mah (1962) determined the standard molal enthalpy of valentinite formation directly from the combustion of valentinite in an oxygen bomb calorimeter:

$$\Delta_f H^\circ_{298,\,Sb_2O_3(valentinite)} = -169.4 \pm 0.7\ kcal{\cdot}mol^{-1}.$$

Combining this value with the entropy for valentinite adopted in this study (29.43 cal·mol−^{1}·K^{-1}), yields the Gibbs energy of formation for valentinite:

$$\Delta_f G^\circ_{298,\,Sb_2O_3(valentinite)} = -149.845 \pm 0.8\ kcal{\cdot}mol^{-1}.$$

3. A series of high-temperature electromotive force (EMF) studies that used the solid-state galvanic cell technique has determined the free energy of formation of valentinite. The extrapolation of $\Delta_f G^\circ_{T,Sb_2O_3(valentitite)}$ obtained by Chatterji and Smith (1973), Azad et al. (1986), Katayama et al. (1987), and Knauth and Schwitzgebel (1988) from the temperature of valentinite-senarmontite phase transition (879 K) to the standard temperature by using the values of S° and C°_p(T) adopted in this study yields values of $\Delta_f G^\circ_{298,Sb_2O_3(valentinite)}$ of −150.518 ± 0.4; −149.203 ± 0.2; −149.950 ± 0.1, and −149.263 ± 1.2, respectively. The EMF measurements made by E. Osadchii (Appendix 3) yield a value of −149.6 ± 0.5 kcal·mol^{-1}. The average value of $\Delta_f G^\circ_{298,Sb_2O_3(valentinite)}$ obtained by using this method (Chatterji and Smith, 1973; Azad et al., 1986; Katayama et al., 1987; Knauth and Schwitzgebel, 1988; and Appendix 3) is −149.7 ± 0.6 kcal·mol^{-1}.

We have opted to use the average $\Delta_f G^\circ_{298,Sb_2O_3(valentinite)}$ value of −149.6 ± 0.3 from the studies discussed above. Note that this value is in excellent agreement with the values presented

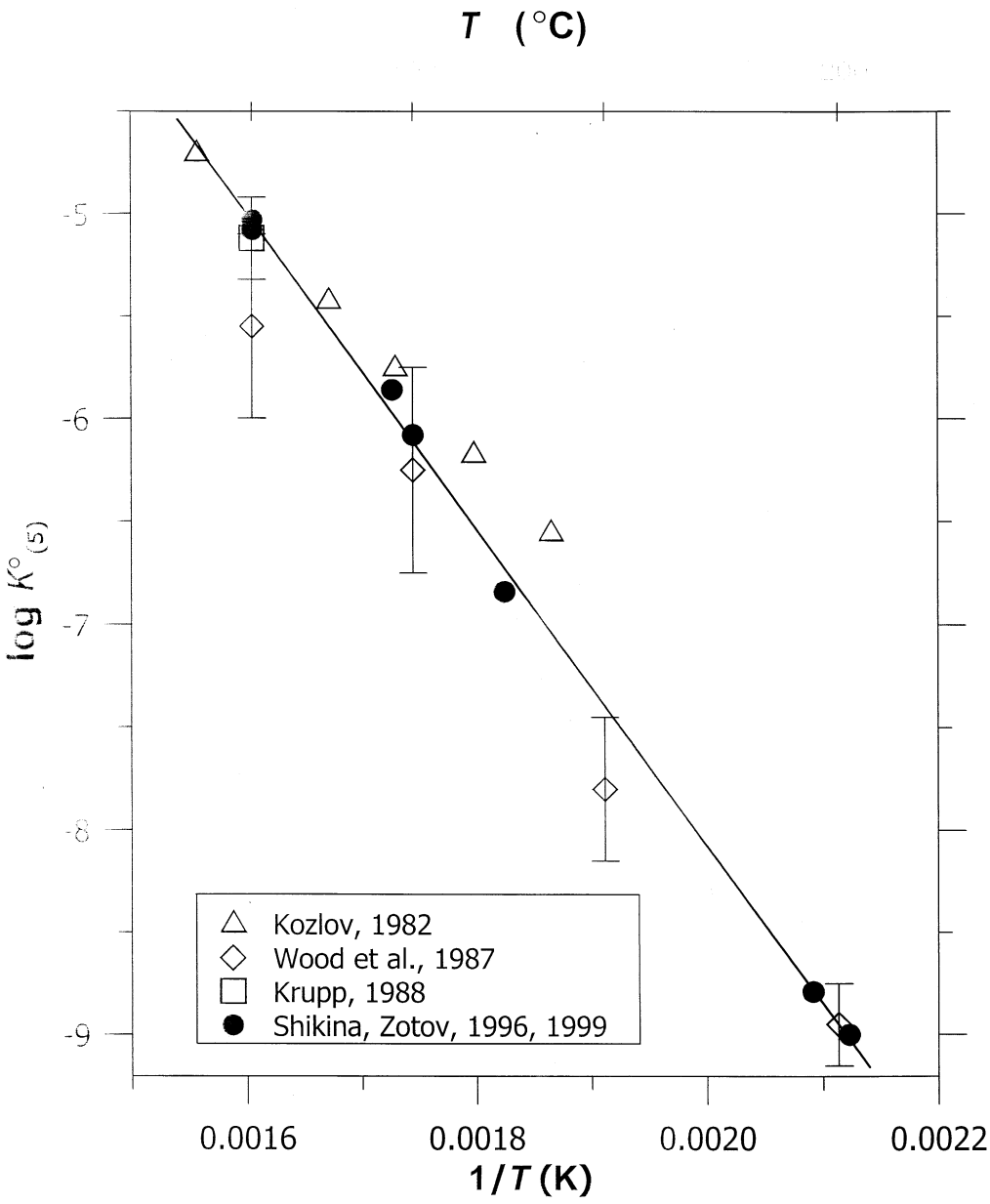

Fig. 7. Log $K°_{(5)}$ as a function of reciprocal temperature at P_{sat} and 500 bars. The symbols denote experimental data; the line represents a linear regression of the data from Shikina and Zotov (1996, 1999).

by Wagman et al. (1982) (−149.74 kcal·mol^{-1}), Pankratz (1982) (−149.76 kcal·mol^{-1}), and Glushko (1968) (−149.48 kcal·mol^{-1}) and close to that given by the IVTANTERMO database (Iorish et al., 1998) (−150.26 kcal·mol^{-1}).

3.2. Senarmontite (Sb_2O_3, cub)

The low-temperature heat capacity of senarmontite has been measured only by Gorgoraki and Tarasov (1965). Although this study seems to have a systematic error (see above), we assumed that the differences between $C°_{p,298}$ and $S°_{298.15}$ values for valentinite and senarmontite (Gorgoraki and Tarasov, 1965) were correct. Then, by use of the data of Behrens and Rosenblatt (1973) for valentinite, we obtain for senarmontite:

$$C°_{p,298} = 22.54 \text{ cal·mol}^{-1}\text{·K}^{-1},$$

$$S°_{298} = 27.37 \text{ cal·mol}^{-1}\text{·K}^{-1}.$$

The heat capacities of senarmontite above 298 K were estimated by the 3*Rn* code (Gurevich et al., 1997). Values of the molal heat capacity of senarmontite in the temperature interval 250 to 300 K were derived as above: from Anderson's data (Anderson, 1930) for valentinite and the difference in $C°_p$ be-

Table 5. $\Delta G^0_{(9),\ 298}$ for polymorphic transformation 9 determined by different methods.

$\Delta G^0_{298,\ (9)}$ (cal·mol^{-1})	Method	Reference
-1740 ± 600[a]	Calculation based on the temperature of phase equilibrium transition	Our recalculation from White et al. (1967)
-1800 ± 200	Potentiometric method	Roberts and Fenwick (1928)
-1230 ± 400[a]	Calculation based on the difference in solubility of senarmontite and valentinite at 80°C ($\Delta G^0_{(9),353.15} = -1.1 \pm 0.3$ kcal·mol^{-1})	Our calculation (Table A1)
-1900 ± 600	Calculation based on the difference in solubility of valentinite at 25°C ($\log K_{(1)} = -4.28$) and that for senarmontite estimated using the extrapolation of solubility data at 80–350° ($\log K_{(2)} = -4.98$)	Gayer and Garrett (1952); our calculation based on Eqn. 3 in this study
15[b]	Heat of dissolution of senarmontite and valentinite in HCl at room temperature	Guntz (1884)[c]
-400[a]	Measurement of saturated vapor pressure of senarmontite and valentinite at 470–640°C ($\Delta H^0_{(9),\ 470-640} = -1.6$ kcal·mol^{-1})	Hincke (1930)
1100[a]	Measurement of saturated vapor pressure of senarmontite and valentinite at 657–1063°C ($\Delta H^0_{(9),\ 657-1063} = -0.1$ kcal·mol^{-1})	Jungermann and Plieth (1967)
-1800 ± 500		Adopted in this study

[a] Recalculated to a temperature of 298.15 K using S^0_{298} and C^0_p (T) dependences for senarmontite and valentinite adopted in this study (Table 6).
[b] Calculated using S^0_{298} values for senarmontite and valentinite adopted in this study (Table 6).
[c] Cited from Popova et al. (1975).

tween valentinite and senarmontite (Gorgoraki and Tarasov, 1965) at the same temperatures. The extrapolated C°_p values in the temperature range from 290 K to the melting point of Sb_2O_3 (928 K) were fitted by the Maier-Kelley equation:

$$C^\circ_{p,\ Sb_2O_3,\ senarmontite}\ (\text{cal·mol}^{-1}\text{·K}^{-1} = 22.525 + 12.028 \times 10^{-3} \times T - 3.179 \times 10^5 \times T^{-2}. \quad (8)$$

The standard Gibbs free energy of formation of senarmontite can be derived by using the free energy change of the reaction of polymorphic transition:

$$Sb_2O_{3(valentinite)} = Sb_2O_{3(senarmontite)}. \quad (9)$$

However, there is a large scatter in $\Delta G^\circ_{298,(9)}$ values obtained by different methods (Table 5). We prefer the method based on the temperature of polymorphic transformation and the ΔS°_{298} and $\Delta C^\circ_p(T)$ data for this reaction. This temperature was accurately determined by White et al. (1967) and is equal to 879 ± 5 K at 1 bar. At this temperature $\Delta G^\circ_{879,(9)} = 0$. By using S° and $C^\circ_p(T)$ for valentinite and senarmontite from Table 6, we calculated the values of $\Delta G^\circ_{298,(9)}$ as -1740 cal·mol^{-1} and $\Delta H^\circ_{298,(9)}$ as -2354 cal·mol^{-1}. The uncertainty in $\Delta S^\circ_{(9)}$ does not exceed 1 cal·mol^{-1}·K^{-1}, which corresponds to an error in $\Delta G^\circ_{298,(9)}$ of ~600 cal·mol^{-1}. The calculated $\Delta G^\circ_{298,(9)}$ value (-1740 ± 600 cal·mol^{-1}) agrees perfectly with that generated by Roberts and Fenwick (1928), who used a potentiometric method ($\Delta G^\circ_{298,(9)} = -1800 \pm 200$ cal·mol^{-1}) and is close to values estimated from the solubility data (Table 5). Calculation based on the solubility data for senarmontite and valentinite at 80°C (Appendix 1, Table A1) and after recalculation of $\Delta G^\circ_{323,(9)}$ to the standard temperature of 298.15 K yields -1230 ± 400 cal·mol^{-1}. Calculation based on the value of solubility of valentinite at 25°C given by Gayer and Garrett (1952) and that for senarmontite estimated by Eqn. 3 (Fig. 3) leads to $\Delta G^\circ_{298,(9)} = -1900 \pm 600$ cal·mol^{-1}. As a result, the average value of ΔG°_{298} from the four values cited above for reaction 9 with regard to uncertainties (Table 5) has been adopted in this study: $\Delta G^\circ_{298,(9)} = -1800 \pm 500$ cal/mol. Values of $\Delta G^\circ_{298,(9)}$ (Table 5) based on the studies of Guntz (1884), Hincke (1930), and Jungermann and Plieth (1967) were ignored. Note that Hincke (1930) and Jungermann and Plieth (1967) used similar methods but obtained contradictory results (Table 5).

Finally, by using the adopted value of $\Delta G^\circ_{298,(9)}$, the stan-

Table 6. Thermodynamic properties of antimony solid phases used in this study.

Solid phases	$\Delta_f G^0_{298,15}$ (kcal·mol^{-1})	$\Delta_f H^0_{298,15}$ (kcal·mol^{-1})	$S^0_{298,15}$ (cal·mol^{-1}·K^{-1})	$V^0_{298,15}$ (cm^3·mol^{-1})	$C^0_{p,298,15}$ (cal·mol^{-1}·K^{-1})	Heat capacity equation (temperature interval in K)
Valentinite (rhombic Sb_2O_3)	-149.6 ± 0.3[a]	-169.3[a]	29.43[c]	50.01 ± 0.06[d]	24.29[c]	$24.841 + 0.0102 \times T - 319700 \times T^{-2}$ (290–928)[a]
Senarmontite (cubic Sb_2O_3)	-151.4 ± 0.6[a]	-171.7[a]	27.37[a]	52.21 ± 0.03[d]	22.54[a]	$22.525 + 0.012028 \times T - 317900 \times T^{-2}$ (290–879)[a]
Stibnite (rhombic Sb_2S_3)	-35.846 ± 0.502[b]	-36.174 ± 0.550[b]	43.50 ± 0.81[b]	73.414 ± 0.05[d]	28.60[b)]	$39.699 - 0.000741 \times T + 154158.7 \times T^{-2} - 217.73 \times T^{-0.5}$ (298–829)[b,e]

[a] This study.
[b] Seal et al. (1992).
[c] Behrens and Rosenblatt (1973).
[d] Naumov et al. (1971).
[e] or $28.8549 + 3.73 \cdot 10^{-3} T - 1.27 \cdot 10^5 T^{-2}$ (the Maier-Kelley equation).

dard Gibbs free energy of formation of senarmontite can be calculated (Table 6):

$$\Delta_f G^\circ_{298,Sb_2O_3(senarmontite)} = \Delta_f G^\circ_{298,Sb_2O_3(valentinite)} + \Delta G^\circ_{298,(9)} = (-149.6 \pm 0.3) + (-1.8 \pm 0.3) = -151.4 \pm 0.6 \text{ kcal·mol}^{-1}.$$

3.3. Stibnite (Sb_2S_3)

The thermodynamic properties of stibnite are discussed in detail by Seal et al. (1992). In spite of large variations in reported values for $\Delta_f H^\circ_{298}$ and $\Delta_f G^\circ_{298}$ of stibnite, these authors have generated a reliable set of thermodynamic properties for this mineral by using low- temperature (Romanovskii and Tarasov, 1960; King and Weller, 1962) and high-temperature (Seal et al., 1992) heat capacity measurements and high-temperature experimental data on the sulfidation of native antimony (Schenck and von der Forst, 1939; Barton, 1971). In this article, we have employed the full set of thermodynamic properties of stibnite reported by Seal et al. (1992) (Table 6).

4. THERMODYNAMIC PROPERTIES OF $SB(OH)_{3(AQ)}$

The values of $\Delta_f G^\circ_{Sb(OH)_{3(aq)}}(P, T)$ were generated for a wide range of temperatures (15 to 450°C) and pressures (1 to 1000 bars) from the solubility data corresponding to reactions 1, 2, 4, and 5 presented in Tables 1 to 4. Activities of the solids and H_2O, and the activity coefficients of the neutral aqueous species were assumed to be unity. Thermodynamic properties of H_2O were calculated by using the equation of state of Hill (1990). Thermodynamic properties of $H_2S_{(aq)}$ were generated by using a new equation of state reported by Akinfiev and Diamond (2003). This approach provides an accurate description of the properties of dissolved gases for a wide range of temperatures (0 to 600°C) and pressures (1 to 4000 bar), and is discussed briefly in Appendix 4.

To estimate the value of the Born parameter for $Sb(OH)_{3(aq)}$, special experiments on senarmontite solubility in H_2O-N_2 supercritical mixed fluids were carried out (Appendix 5). The Born parameter was extracted by the algorithm given by Akinfiev and Zotov (1999). It is based on the electrostatic interaction between dissolved species and the surrounding molecules of H_2O. According to this approach, the logarithm for the equilibrium constant of a reaction is expressed as

$$\Delta \log K^0 = -\Delta_r\omega \times \Theta, \tag{10}$$

where $\Delta\log K^\circ$ denotes the deviation of $\log K^\circ$ in the mixture relative to that in pure H_2O, $\Delta_r\omega$ is the change in the Born parameter for the reaction, and Θ denotes the "dielectric correction factor" as follows:

$$\Theta = \left(\frac{1}{\epsilon} - \frac{1}{\epsilon_{H_2O}}\right) \times \frac{1}{2.303RT}, \tag{11}$$

where ε and ε_{H_2O} correspond to the dielectric permittivity of the mixture and pure water, respectively, and R and T represent the universal gas constant and absolute temperature in K, respectively. For reaction 2, $\Delta_r\omega$ is identical to $\omega_{Sb(OH)_{3(aq)}}$, and hence the value for the Born parameter of $Sb(OH)_{3(aq)}$ can be calculated from the decrease in senarmontite solubility with increasing mole fraction of N_2. The experimental data, calculated values of dielectric permitivity, and dielectric correction factor are presented in Table A5. The dependence of $\log K^\circ_{(2)}$ on the dielectric correction factor is shown in Fig. A5. By use of the linear slope of the relationship, we obtain $\omega_{Sb(OH)_{3(aq)}} = (0.046 \pm 0.003)\cdot 10^5$ cal·mol^{-1}.

Volumetric properties of $Sb(OH)_{3(aq)}$ were extracted by using the dependence of senarmontite solubility on pressure at temperatures of 210°C and 300°C (Table 2) The standard chemical potential of $Sb(OH)_{3(aq)}$ can be expressed as

$$\mu^\circ_{Sb(OH)_{3(aq)}} = 0.5\mu^\circ_{sen.} + 1.5\mu^\circ_{H_2O} - RT \ln m_{Sb(OH)_{3(aq)}}, \tag{12}$$

where $m_{Sb(OH)_{3(aq)}}$ is the measured molal concentration of Sb, and $\mu^\circ_{sen.}$ and $\mu^\circ_{H_2O}$ represent the standard chemical potentials of senarmontite and water at the temperature and pressure of interest. Values of $\mu^\circ_{sen.}$ and $\mu^\circ_{H_2O}$ were calculated by using data from Table 6 and the SUPCRT92 computer package (Johnson et al., 1992). Then, by use of the common thermodynamic expression

$$V = \left.\frac{\partial \mu^\circ}{\partial P}\right|_T \approx \frac{\mu^\circ_{P_1} - \mu^\circ_{P_2}}{P_1 - P_2}, \tag{13}$$

the average values of molal $Sb(OH)_{3(aq)}$ volume in a range of pressure from vapor saturated pressure to 1000 bars were derived: 52 ± 7 and 56 ± 5 cm^3·mol-1 at 210° and 300°C, respectively. The value of $V_{Sb(OH)_{3(aq)}}$ for standard state conditions (25°C and 1 bar) was matched by using values of $V_{Sb(OH)_{3(aq)}}$ calculated above at 210°C and 300°C and correlation algorithms for the volumetric HKF parameters (a_1, a_2, a_3, and a_4) from Shock et al. (1989). The derived value of the standard partial molal volume of $Sb(OH)_{3(aq)}$ $V^\circ_{298,Sb(OH)_3(aq)}$ is equal to 54 ± 7 cm^3·mol^{-1}.

Taking account of the derived V°_{298} and ω_{298} for $Sb(OH)_{3(aq)}$, the values of $\Delta_f G^\circ_{Sb(OH)_{3(aq)}}(P, T)$ generated above were regressed by the UT-HEL code of the HCH software package (Shvarov, 1999; Shvarov and Bastrakov, 1999) consistent with the revised HKF equation of state (Tanger and Helgeson, 1988). Two parameters were used in the optimization procedure: S°_{298} and $C^\circ_{p,298}$. The heat capacity HKF parameters c_1 and c_2 were derived by the correlation from Shock et al. (1989).

The generated standard molal thermodynamic properties of $Sb(OH)_{3(aq)}$ at 25°C and 1 bar and the corresponding HKF parameters are given in Table 7. The difference between the experimental $Sb(OH)_{3(aq)}$ Gibbs free energy values and those predicted by these parameters is shown in Figure 8. This difference is equal to ~0.25 kcal·mol^{-1} at 25°C and increases with temperature to 0.5 to 0.6 kcal·mol^{-1} at 450°C. Thus, the uncertainty in the predicted constants of reactions 1 to 5 does not exceed 0.2 log units for the range of temperature and pressure considered in this study.

5. APPLICATION TO NATURAL SYSTEMS

The stability of minerals in the system Fe-Sb-S-O-H and the principal factors that control antimony transport and deposition were recently considered in detail by Williams-Jones and Normand (1997). Here we will briefly discuss the relative stability of hydroxy and bisulfide antimony species using the new ther-

Table 7. Standard thermodynamic properties and HKF parameters of $Sb(OH)_{3(aq)}$ adopted in this study.

Thermodynamic parameters		$Sb(OH)_{3(aq)}$
$\Delta_f G^0_{298}$	(cal·mol^{-1})	−154,010
S^0_{298}	(cal·mol^{-1}·K^{-1})	43.260
$C^0_{p.\,298}$	(cal·mol^{-1}·K^{-1})	66.4
V^0_{298}	(cm^3·mol^{-1})	54.0
$a_1 \cdot 10$	(cal·mol^{-1}·bar^{-1})	9.1718
$a_2 \cdot 10^{-2}$	(cal·mol^{-1})	14.6130
a_3	(cal·K·mol^{-1}·bar^{-1})	0.0064
$a_4 \cdot 10^{-4}$	(cal·K·mol^{-1})	−3.3831
c_1	(cal·mol^{-1}·K^{-1})	45.5017
$c_2 \cdot 10^{-4}$	(cal·K·mol^{-1})	10.4911
$\omega \cdot 10^{-5}$	(cal·mol^{-1})	0.0461

modynamic data for $Sb(OH)_{3(aq)}$ generated in this study and thermodynamic data for antimony species in sulfide solutions calculated by Akinfiev et al. (1993).

The most comprehensive experimental investigation of stibnite solubility in sulfide solutions was carried out by Krupp (1988), who concluded that at high temperatures (300 to 350°C), the predominant Sb species is $Sb_2S_2(OH)_{2(aq)}$. However, the data presented above (section 2.3; Figs. 5 and 6) show that at these temperatures the hydroxide species $Sb(OH)_{3(aq)}$ dominates at H_2S concentrations up at least to 0.1*m*. Consequently, the data of Krupp (1988) need to be reinterpreted to take account of the hydroxide species at high temperatures (200 to 350°C). Such a reinterpretation was performed by Akinfiev et al. (1993). The further revision of stoichiometry and stability of sulfide Sb species (Belevantsev et al., 1998b; Gushchina et al., 2000) applied only to highly alkaline solutions.

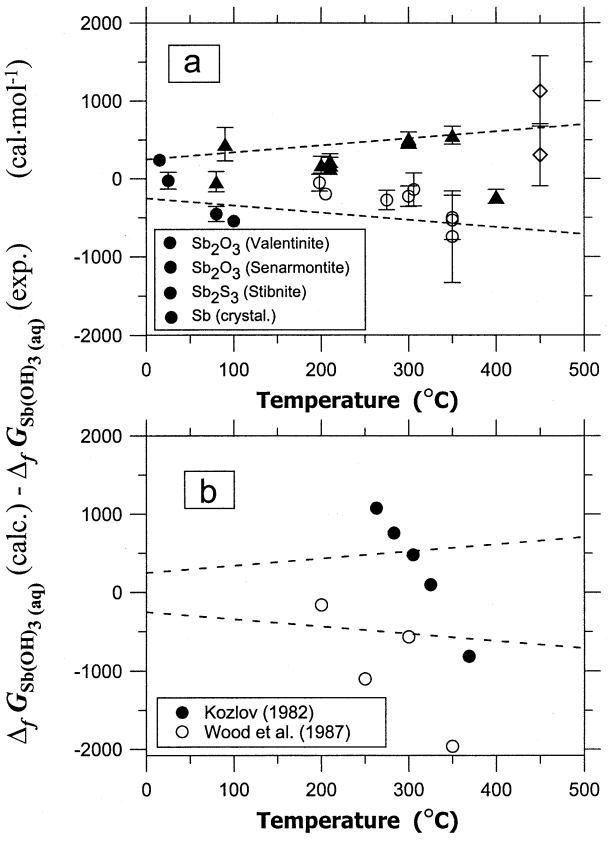

Fig. 8. Differences between calculated values of Gibbs energy of $Sb(OH)_{3(aq)}$ by using the data from Table 7 and those generated from experimental measurements (Tables 1 to 4). The dashed lines correspond to the error of ± 0.2 in log *K*.

In our analysis of the behavior of Sb in natural systems, the thermodynamic properties of Sb sulfide complexes and $Sb(OH)_4^-$ are taken from Akinfiev et al. (1993). Data for $Sb(OH)_{3(aq)}$, stibnite, and $H_2S_{(aq)}$ are given in Tables 7, 6, and A4 of this study, respectively. The thermodynamic properties for other aqueous species (HS^-, OH^-, Na^+, Cl^-, $NaCl_{(aq)}$, $NaOH_{(aq)}$, $O_{2(aq)}$, $H_{2(aq)}$) and solid phases (pyrite, pyrrhotite, magnetite) used in our calculations were taken from SUPCRT92 (Johnson et al., 1992). Activity coefficients of charged species were calculated by the extended Debye-Hückel equation with a value of $\mathring{a} = 4.5 \times 10^{-8}$ cm adopted for all species. Activity coefficients of neutral aqueous species were assumed to be unity.

The fields of predominance of the various Sb species are shown in Figure 9 at temperatures of 25, 100, 200, and 350°C and saturated vapor pressure. The stability field of stibnite is given at a total Sb concentration equal to $10^{-6}m$ (Fig. 9A) and $10^{-4}m$ (Fig. 9B), and an ionic strength of 0.1 at all temperatures.

Figure 9 demonstrates that increasing temperature rapidly reduces the stibnite stability field and widens the field of predominance of $Sb(OH)_{3(aq)}$ relative to sulfide Sb species. The deposition of stibnite in natural environments is virtually impossible at high temperature (above 350°C) because of the very high solubility of this mineral in H_2O (up to $10^{-2}m$ Sb). The strong increase of stibnite solubility with increasing temperature leads to the conclusion that decreasing temperature is one of the most important factors in antimony deposition. At lower temperatures, antimony can be transported both as $Sb(OH)_{3(aq)}$ and bisulfide complexes ($H_2Sb_2S_{4(aq)}$, $HSb_2S_4^-$ and $Sb_2S_4^{2-}$). Hence, Sb speciation in natural fluids depends on the H_2S concentration. At low H_2S concentration, Sb is transported as $Sb(OH)_{3(aq)}$. This speciation is evident for natural chemical conditions encountered during modern stibnite formation in the Uzon geothermal system, Kamchatka (Alekhin et al., 1987): $\Sigma m_{Sb} \approx 2 \cdot 10^{-6}$ to 5×10^{-5} mol·kg^{-1}; $T \approx 93$ to 98°C. Symbols in Figures 9A,B represent the measured in situ pH and H_2S concentrations in natural solutions with coexisting stibnite. Our calculations show that at high temperature (200 to 350°C), $Sb(OH)_{3(aq)}$ is also the main agent in the transport of Sb if the H_2S concentration is buffered by the pyrite + pyrrhotite + magnetite assemblage (dashed line in Fig. 9). However, many researchers (Barnes, 1979; Sorokin et al., 1988) have proposed, on the basis of a study of fluid inclusions, markedly higher concentrations (up to 10^{-1} mol·kg^{-1}) of H_2S in ore fluids. For example, Kolpakova (1982b) determined that the H_2S concentration ranged from 10^{-1} to 10^{-3} mol·kg^{-1} in fluid inclusions from low-temperature Dzhizhikrut hydrothermal Sb deposit, Tadjikistan, and low-temperature Au-Sb deposits in Yakutiya. In these situations, Sb is likely to be transported as sulfide species. The type of Sb speciation (hydroxide vs. sulfide complexes) will determine the effect of variations in the H_2S concentration on ore deposition. Deposition of stibnite is associated with an increase in the H_2S

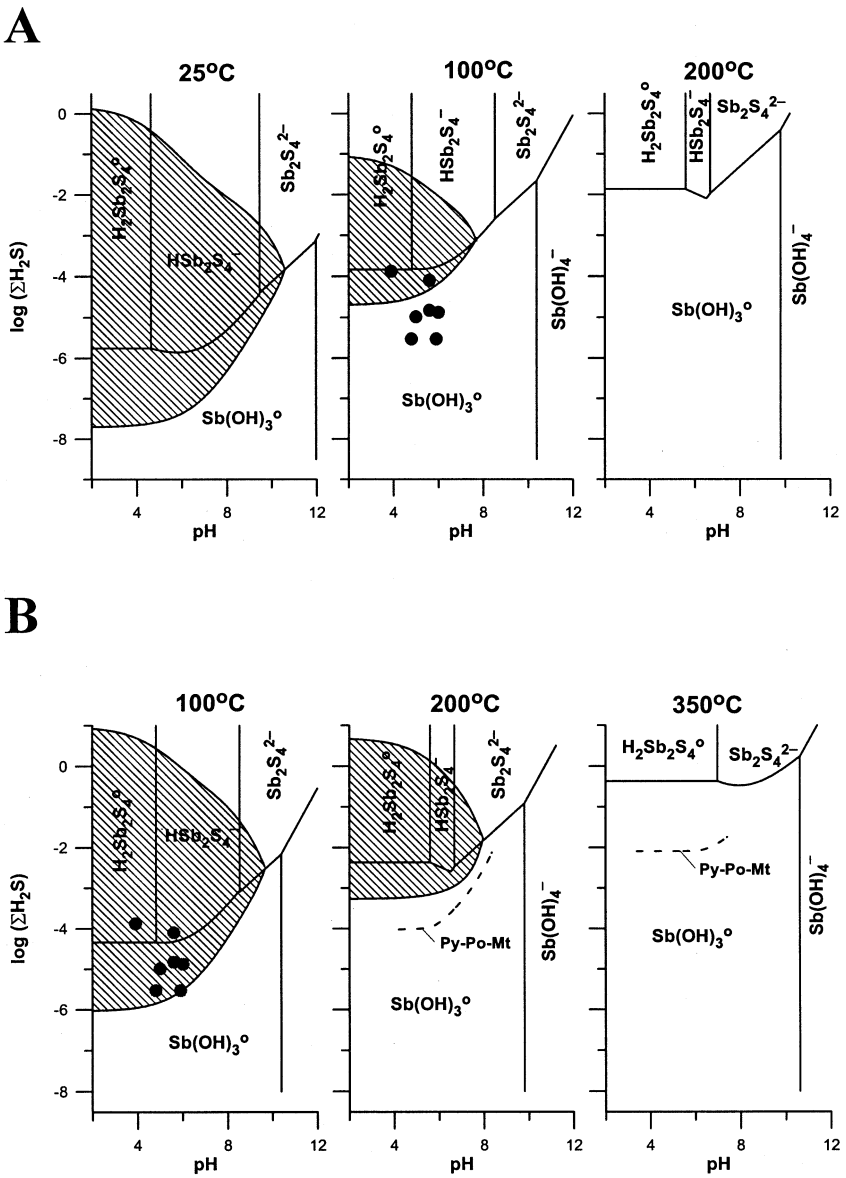

Fig. 9. Plots of log $m_{(H_2S+HS^-)}$ vs. pH at 25, 100, 200, and 350°C, showing the fields of predominance of Sb-bearing species. The shaded areas show the stability field of stibnite. The total Sb concentration is 10^{-6} mol·kg^{-1} (A) and 10^{-4} mol·kg^{-1} (B), and the ionic strength of the fluid is 0.1. Solid circles indicate conditions measured by Alekhin et al. (1987) for the natural fluid from the Uzon caldera, Kamchaka. The dashed lines correspond to the equilibrium conditions for the pyrite + pyrrhotite + magnetite buffer association (at an ionic strength of approximately 0.15) calculated with the GIBBS code for the HCH software package (Shvarov, 1999; Shvarov and Bastrakov, 1999).

concentration if $Sb(OH)_{3(aq)}$ dominates in the fluid, and with a decrease in H_2S if Sb is present as sulfide species.

6. CONCLUSION

We have attempted to summarize all the available data relating to the stability of $Sb(OH)_{3(aq)}$ at elevated temperatures and pressures and have used these data to derive standard thermodynamic properties and HKF parameters for $Sb(OH)_{3(aq)}$ that are consistent with thermodynamic properties for the solid antimony phases (Sb, Sb_2O_3, Sb_2S_3). Both experimental data and thermodynamic calculations confirm that the hydroxide complex $Sb(OH)_{3(aq)}$ is primarily responsible for the hydrothermal transport of antimony, especially at temperatures above 200 to 250°C.

Acknowledgments—This research was supported by the Russian Foundation of Fundamental Investigations, grants 98-05-64234 and 00-05-64211. We thank V. Popolitov and L. Demyanets for supplying synthetic senarmontite and valentinite, and we thank B. Manachyuryants for natural senarmontite. We thank I. L. Khodakovsky for helpful discussions during the course of this study and for providing us with the computer program 3*Rn*. We are grateful to G. Pokrovski for supplying unpublished XAFS data and correcting the English-language version of the article in manuscript. We also thank Yu. Shvarov for providing his

computer code UT-HEL. We are very grateful to E. Osadchii, who carried out the experimental EMF measurements, and to M. Drushits and M. Voronin for their help in solubility experiments with H_2O-N_2 mixtures. Special thanks to K. V. Ragnarsdottir for her review of a previous version of the article in manuscript. Constructive reviews by A. E. Williams-Jones, J. Schott, and an anonymous reviewer led to significant improvements to the text.

Associate editor: K. Ragnarsdottir

REFERENCES

Akeret R. (1953) Über die Löslichkeit von Antimon (3) Sulfid. Ph.D. thesis, Eidgenössische Technische Hochschule, Zürich (Prom. N 2271).

Akinfiev N. N. (1997) Thermodynamic description of H_2O-gas binary systems by means of Redlich-Kwong equation over a wide range of parameters of state. *Geochem. Int.* **35,** 188–196.

Akinfiev N. N. and Diamond L. W. (2003) Thermodynamic description of aqueous non-electrolytes at infinite dilution over a wide range of state parameters. *Geochim. Cosmochim. Acta* **67,** 613–627.

Akinfiev N. N., Zotov A. V., and Shikina N. D. (1993) Experimental investigations and fitting of thermodynamic data in the system Sb(III)-S(II)-O-H (in Russian). *Geokhimiya*, **N12,** 1709–1723.

Akinfiev N. and Zotov A. (1999) Thermodynamic description of equilibria in mixed fluids (H_2O–non-polar gas) over a wide range of temperature (25–700°C) and pressure (1–5000 bars). *Geochim. Cosmochim. Acta* **63,** 2025–2042.

Alekhin Yu. V., Dadze T. P., Zotov A. V., Karpov G. A., Sorokin V.I., and Mironova G. D. (1987) Conditions of formation for modern sulfide Hg-Sb-As ore mineralization in Uzon caldera (Kamchatka) (in Russian) *Vulkanol. Seysmol.* **N2,** 34–43.

Anderson C. T. (1930) The heat capacities at low temperatures of antimony, antimony trioxide and antimony pentoxide. *J. Am. Chem. Soc.* **52,** 2712–2720.

Arnston R. H., Dickson F. W., and Tunnel G. (1966) Stibnite (Sb_2S_3) solubility in sodium sulfide solutions. *Science* **153,** 1673–1674.

Azad A. M., Pankajavalli R., and Sreedharan O. M. (1986) Thermodynamic stability of Sb_2O_3 by a solid-oxide electrolyte e.m.f. technique. *J. Chem. Thermodynam.* **18,** 255–261.

Babko A. K. and Lisetskaya G. S. (1956) Equilibrium in reactions of formation of thiosalts of tin, antimony, and arsenic in solution (in Russian). *J. Inorg. Chem.* **1,** 969–980.

Barbero J. A., McCurdy K. G., and Tremaine P. R. (1982) Apparent molal heat capacities and volumes of aqueous hydrogen sulfide and sodium hydrogen sulfide near 25°C: The temperature dependence of H_2S ionization. *Can. J. Chem.* **60,** 1872–1880.

Barnes H. L. (1979) Solubility of ore minerals. In *Geochemistry of Hydrothermal Ore Deposits*, 2nd ed. (ed. H. L. Barnes), pp. 404–406. Wiley-Interscience.

Barton P. B. Jr (1971) The Fe-Sb-S system. *Econ. Geol.* **66,** 121–132.

Behrens R. G. and Rosenblatt G. M. (1973) Vapor pressure and thermodynamics of orthorhombic antimony trioxide (valentinite). *J. Chem. Thermodyn.* **5,** 173–188.

Belevantsev V. L., Gushchina L. V., and Obolenskii A. A. (1998a) Antimony in hydrothermal solutions: Analysis and generalization of data on antimony (III) chloride complexes. *Geochem. Int.* **36,** 928–933.

Belevantsev V. L., Gushchina L. V., and Obolenskii A. A. (1998b) Solubility of stibnite, $Sb_2S_{3(cr)}$: A revision of proposed interpretations and refinements. *Geochem. Int.* **36,** 58–64.

Chang S. S. and Bestul A. B. (1971) Heat capacities of cubic, monoclinic, and vitreous arsenious oxide from 5 to 360 K. *J. Chem. Phys.* **55,** 933–946.

Chatterji D. and Smith J. V. (1973) Free energy of formation of Bi_2O_3, Sb_2O_3 and TeO_2 from EMF measurements. *J. Electrochem. Soc.* **120,** 889–893.

Clarke E. C. W. and Glew D. N. (1971) Aqueous nonelectrolyte solutions. Part VIII. Deuterium and hydrogen sulfides solubilities in deuterium oxide and water. *Can. J. Chem.* **49,** 691–698.

Drummond S. E. (1981) Boiling and mixing of hydrothermal fluids: Chemical effects of mineral precipitation. Ph.D. thesis, Pennsylvania State University.

Fredriksson M. A. and Rosén E. (1984) Thermodynamic studies of high temperature equilibria 28. Solid state EMF studies of the sulfide-oxide equilibrium in the system Sn-S-O. *Scand. J. Metal.* **13,** 95–97.

Gayer K. H. and Garrett A. B. (1952) The equilibria of antimonous oxide (rhombic) in dilute solutions of hydrochloric acid and sodium hydroxide at 25°. *J. Am. Chem. Soc.* **74,** 2353–2354.

Glushko V. P. (ed.) (1968) *Thermal Constants of Substances* (in Russian). Vol. 3. VINITI Press.

Gorgoraki E. A. and Tarasov V. V. (1965) Low temperature heat capacities and some thermodynamic properties of As and Sb trioxides (in Russian). *Trudy Mosk. Khim. Tekhnol. Inst.* **49,** 11–15.

Guntz A. P. (1884) Sur le fluorure d'antimoine. *C. R. Acad. Sci.* **98,** 303.

Gurevich V. M., Sergeeva E. I., Gavrichev K. S., Gorbunov V. E., Kuznetsova T. P., and Khodakovskii I. L. (1997) Thermodynamic properties of uranyl hydroxide $UO_2(OH)_2$ (cr, α, rhomb). *Geochem. Int.* **35,** 74–87.

Gushchina L. V., Borovikov A. A., and Shebanin A. P. (2000) Formation of antimony (III) complexes in alcali sulfide solutions at high temperatures: An experimental Raman spectroscopic study. *Geochem. Int.* **38,** 510–513.

Hill P. G. (1990) A unified fundamental equation for the thermodynamic properties of H_2O. *J. Phys. Chem. Ref. Data* **19,** 1233–1274.

Hincke W. B. (1930) The vapor pressure of antimony trioxide. *J. Am. Chem. Soc.* **52,** 3869–3877.

Hnědkovsky L., Wood R. H., and Majer V. (1996) Volumes of aqueous solutions of CH_4, CO_2, H_2S, and NH_3 at temperatures from 298.15 K to 705 K and pressures to 35 MPa. *J. Chem. Thermodyn.* **28,** 125–142.

Hnědkovsky L. and Wood R. H. (1997) Apparent molar heat capacity of aqueous solutions of CH_4, CO_2, H_2S, and NH_3 from 304 K to 704 K at 28 MPa. *J. Chem. Thermodyn.* **29,** 731–747.

Iorish V. S., Belov G. V., Yungman V. S. (1998) IVTANTHERMO for Windows and its use for the applied thermodynamic analysis. Preprint 8-415. Joint Institute for High Temperature of the Russian Academy of Sciences.

Johnson J. W., Oelkers E. H., and Helgeson H. C. (1992) SUPCRT92: A software package for calculating the standard molal thermodynamic properties of minerals, gases, aqueous species, and reactions from 1 to 5000 bars and 0° to 1000°C. *Comp. Geosci.* **18,** 899–947.

Jungermann E. and Plieth K. (1967) Dampfdrucke und Kondensationgeschwindigkeiten der polymorphen Arsen- und Antimontrioxide. *Z. Phys. Chem. (BRD)* **53,** 215.

Karpov G. A. (1988) *The Present-Day Hydrotherms and Mercury–Antimony–Arsenic Ore Mineralisation* (in Russian). Nauka.

Katayama J., Sugimura S., and Kozuka Z. (1987) Measurements of standard molar Gibbs energies of formation of Sb_2O_3, $ZnSb_2O_4$ and $MgSb_2O_4$ by EMF method with zirconia solid electrolyte. *Trans. Jap. Inst. Metals* **28,** 406–411.

King E. G., and Weller W. W. (1962) Low-temperature heat capacities and entropies at 298.15K of antimony and indium sulfides. Report Investigations. 6040. U.S. Bureau of Mines.

Kishima N. (1989) A thermodynamic study on the pyrite-pyrrhotite-magnetite-water system at 300–500°C with relevance to the fugacity/concentraton quotient of aqueous H_2S. *Geochim. Cosmochim. Acta* **53,** 2143–2155.

Knauth P. and Schwitzgebel G. (1988) E.m.f. and calorimetric investigations of antimony oxides. *Ber. Bunsenges. Phys. Chem.* **92,** 32–35.

Kolpakova N. N. (1971) On the speciation of antimony (III) in sulfide solutions (in Russian). In *Geochemistry of Hydrothermal Ore Deposition* (ed. V. L. Barsukov), pp. 197–209. Nauka .

Kolpakova N. N. (1982a) Laboratory and field studies of ionic equilibria in the Sb_2S_3-H_2O-H_2S system. *Geochem. Int.* **19,** 46–54.

Kolpakova N. N. (1982b) Determination of hydrogen sulfide in the fluid inclusions of the gangue minerals (in Russian). *Geokhimiya*, **N2,** 271–276.

Kozintseva T. N. (1964) Solubility of hydrogen sulfide in water at elevated temperatures. *Geochem. Int.*, **N1,** 1739–1754.

Kozlov E. D. (1982) Migration of antimony and mercury in hydrothermal solutions based on experimental data (in Russian). Ph.D. thesis, Institute of Mineralogy, Geochemistry and Crystallochemistry of Rare Elements. Moscow.

Krainov S. R., Volkov G. A., and Petrova N. G. (1979) Antimony geochemistry in carbonate waters of the Carpathians in connection with low temperature ore formation (in Russian). *Geokhimiya*, **N10,** 1488–1498.

Krupp R. E. (1988) Solubility of stibnite in hydrogen sulfide solutions, speciation, and equilibrium constants, from 25 to 350°C. *Geochim. Cosmochim. Acta* **52,** 3005–3015.

Krupp R. E. and Seward T. M. (1990) Transport and deposition of metals in the Rotokawa geothermal system, New Zealand. *Min. Dep.* **25,** 73–81.

Learned R. E., Tannel G., and Dickson F. W. (1974) Equilibria of cinnabar, stibnite and saturated solutions in the system HgS-Sb_2S_3-Na_2S-H_2O from 150 to 250°C at 100 bars, with implications concerning ore genesis. *J. Res. U. S. Geol. Surv.* **2,** 457–466.

Mah A. D. (1962) Heats and free energies of formation of antimony sesquioxide and tetroxide. Report Investigations. 5972. U.S. Bureau of Mines.

Mosselmans J. F. W., Helz G. R., Pattrick R. A. D., Charnock J. M., and Vaughan D. J. (2000) A study of speciation of Sb in bisulfide solutions by X-ray spectroscopy. *Appl. Geochem.* **15,** 879–889.

Namiot A. Yu. (1991) *Solubility of Gases in Water* (in Russian). Nedra.

Naumov G. B., Ryzhenko B. N., Khodakovsky I. L. (1971) *Handbook of Thermodynamic Values (for Geologists)* (in Russian). Atomizdat.

Nekrasov I. Ya. and Konyushok A. A. (1982) Heteropolynucleate gold complexes in antimony-bearing sulfide solutions (in Russian). *Dokl. Akad. Nauk SSSR* **267,** 185–188.

O'Connell J. P., Sharygin A. V., and Wood R. H. (1996) Infinite dilution partial molar volumes of aqueous solutes over wide ranges of conditions. *Ind. Eng. Chem. Res.* **35,** 2808–2812.

Oelkers E. H., Sherman D. M., Ragnarsdottir K. V., and Collins C. (1998) An EXAFS spectroscopic study of aqueous antimony (III)-chloride complexation at temperatures from 25 to 250°C. *Chem. Geol.* **151,** 21–27.

Osadchii E., Lunin S., Fed'kin M., Zhdanov N., and Kotova A. (1998) Thermodynamic study of sulphides, intermetallides, and natural processes by solid state electrochemical cell method at high T-P parameters (in Russian). In *Experimental and Theoretical Modelling of the Processes of Mineral Formation*, pp. 355–379. Nauka.

Pankratz L. B. (1982) Thermodynamic properties of elements and oxides. Bulletin 672. U.S. Department of the Interior, Bureau of Mines.

Plyasunov A. V. (1991) The approximate computation of Henry's constants of non polar gases at water supercritical temperatures (in Russian). *Dokl. Ak. Nauk SSSR* **321,** 1071–1074.

Plyasunov A. V., O'Connell J. P., and Wood R. H. (2000) Infinite dilution partial molar properties of aqueous solutions of nonelectrolytes. I. Equations for partial molar volumes at infinite dilution and standard thermodynamic functions of hydration of volatile nonelectrolytes over wide range conditions. *Geochim. Cosmochim. Acta* **64,** 495–512.

Popolitov V. I. (1989) Crystallisation of some metals, metalloids, and simple oxides by hydrothermal techniques (in Russian). *Izvestiya Acad. Nauk USSR, Neorganich. Mater.* **25,** 1681–1684.

Popova M. Ya., Khodakovsky I. L., and Ozerova N. A. (1975) Experimental determination of the thermodynamic properties hydroxo- and hydroxofluoride complexes of antimomy at temperatures up to 200°C (in Russian). *Geokhimiya*, **N6,** 835–843.

Pourbaix M. (1966) *Atlas of Electrochemical Equilibria in Aqueous Solutions.* Brussels.

Roberts E. J. and Fenwick F. (1928) Antimony-antimony trioxide electrode and its use as a measure of acidity. *J. Am. Chem. Soc.* **50,** 2125–2147.

Romanovskii V. A. and Tarasov V. V. (1960) Heat capacity of the trisulfides of arsenic, antimony, and bismuth in connection with their structural and physical-chemical properties. *Sov. Phys. Solid State* **2,** 1170–1175.

Schenck R. and von der Forst P. (1939) Gleichgewichtsstudien an erzbildenden sulfiden II. *Zeitsghr. Anorg. Allgem. Chem.* **241,** 145–157.

Schuhmann R. (1924) Free energy of antimony trioxide and the reduction potential of antimony. *J. Am. Chem. Soc.* **46,** 52–58.

Schulze H. (1883) *J. Prakt. Chem.* **27,** 320.

Seal R. R. II, Robie R. A., Barton P. B. Jr., and Hemingway B. S. (1992) Superambient heat capacities of synthetic stibnite, berthierite, and chalcostibite: Revised thermodynamic properties and implications for phase equilibria. *Econ. Geol.* **87,** 1911–1918.

Shikina N. D. and Zotov A. V. (1990) Thermodynamic properties of $Sb(OH)_3^o$ at temperature up to 723.15 K and pressure 1000 bars (in Russian). *Geokhimiya*, **N12,** 1767–1772.

Shikina N. D. and Zotov A. V. (1996) Stoichiometry of the neutral antimony hydroxo complex (in Russian) *Geokhimiya*, **N12,** 1242–1244.

Shikina N. D. and Zotov A. V. (1999) Solubility of stibnite (Sb_2S_3) in water and hydrogen sulfide solutions at temperature of 200–300°C under vapor-saturated conditions and a pressure of 500 bars. *Geochem. Int.* **37,** 82–86.

Shock E. L., Helgeson H. C., and Sverjensky D. A. (1989) Calculation of the thermodynamic and transport properties of aqueous species at high pressures and temperatures: Standard partial molal properties of inorganic neutral species. *Geochim. Cosmochim. Acta* **53,** 2157–2183.

Shvarov Yu. V. (1999) Algorithmization of the numerical equilibrium modelling of dynamic geochemical processes. *Geochem. Int.* **37,** 571–576.

Shvarov Y. and Bastrakov E. (1999) *A Software Package for Geochemical Equilibrium Modeling: User's Guide.* Australian Geological Survey Organisation, Department of Industry, Science and Resources.

Sorokin V. I., Pokrovskii V. A., and Dadze T. P. (1988) *Physical-Chemical Conditions of Antimony–Mercury Ore Formation.* Nauka.

Spycher N. F. and Reed M. H. (1989) As(III) and Sb(III) sulfide complexes: An evaluation of stoichiometry and stability from existing experimental data. *Geochim. Cosmochim. Acta* **53,** 2185–2194.

Stauffer R. E. and Thompson J. M. (1984) Arsenic and antimony in geothermal waters of Yellowstone National Park, Wyoming, USA. *Geochim. Cosmochim. Acta* **48,** 2547–2561.

Suleimenov O. M. and Krupp R. E. (1994) Solubility of hydrogen sulfide in pure water and in NaCl solutions, from 20 to 320°C and at saturation pressures. *Geochim. Cosmochim. Acta* **58,** 2433–2444.

Tanger J. C. and Helgeson H. C. (1988) Calculation of the thermodynamic and transport properties of aqueous species at high pressure and temperatures: Revised equations of state for the standard partial molal properties of ions and electrolytes. *Am. J. Sci.* **288,** 19–98.

Vasil'ev V. P. and Shorokhova V. I. (1972a) Determination of the standard thermodynamic properties of antimonil ion SbO^+ and antimony trioxide by potentiometric method (in Russian). *Electrokhimiya*, **8,** 185–190.

Vasil'ev V. P. and Shorokhova V. I. (1972b) Determination of the standard thermodynamic properties of antimonil ion SbO^+ by solubility method (in Russian). In *Trudy Ivanovskogo Khimiko-tekhnologicheskogo Instituta*, Vol. 13, pp. 75–80. Ivanovo.

Vasil'ev V. P. and Shorokhova V. I. (1973) Determination of standard thermodynamic properties of antimony (III) in alkaline solutions by solubility method (in Russian). *J. Neorg. Khimii.* **18,** 305–310.

Wagman D. D., Evans W. H., Parker V. B., Schumm R. H., Halow I., Bailey S. M., Churney K. L., and Nuttall R. L. (1982) The NBS tables of chemical thermodynamic properties. Selected values for inorganic and C_1 and C_2 organic substances in SI units. *J. Phys. Chem. Ref. Data* **11**(Suppl. 2), 1–392.

White D. E. (1967) Mercury and base-metal deposits with associated thermal and mineral waters. In *Geochemistry of Hydrothermal Ore Deposits* (ed. H. L. Barnes), pp. 575–626. Holt, Rinehart and Winston.

White W. B., Dachille F., and Roy R. (1967) High-pressure polymorfism of As_2O_3 and Sb_2O_3. *Z. Kristallogr.* **125,** 450–458.

Williams-Jones A. E. and Normand C. (1997) Control of mineral parageneses in the system Fe-Sb-S-O. *Econ. Geol.* **92,** 308–324.

Wood S. A. (1989) Raman spectroscopic determination of ore metals in hydrothermal solutions: I. Speciation of antimony in alkaline sulfide solutions at 25°C. *Geochim. Cosmochim. Acta* **53,** 237–244.

Wood S. A., Crerar D. A., and Borcsik M. P. (1987) Solubility of the assemblage pyrite-pyrrhotite-magnetite-sphalerite-galena-gold-stibnite-bismuthinite-argentite-molybdenite in H_2O-NaCl-CO_2 solutions from 200° to 350°C. *Econ. Geol.* **82,** 1864–87.

Zotov A. V., Kudrin A. V., Levin K. A., Shikina N. D., and Var'yash L. N. (1995) Experimental studies of the solubility and complexing of selected ore elements (Au, Ag, Cu, Mo, As, Sb, Hg) in aqueous solutions. In *Fluids in the Crust: Equilibrium and Transport Prop-*

erties (eds. K. I. Shmulovich, B. W. D. Yardley, and G. G. Gonchar), pp. 95–137. Chapman and Hall.

APPENDIX 1

Valentinite and Senarmontite Solubility in H_2O at 80°C

Dissolution experiments were performed on natural senarmontite from an Algerian deposit and two samples of synthetic valentinite. The first sample (Valentinite-1) is a fine-grained chemical reagent (Sb_2O_3 99.99%). The second sample (Valentinite-2) is characterized by needle-shaped crystals ranging from 3 to 10 mm in length and 0.2 to 0.8 mm in diameter. These crystals were synthesized from pure antimony (III) oxide (Merck) at 450°C in the Institute of Crystallography of the Russian Academy of Sciences by using the fluoride method (Popolitov, 1989). Both solids were analyzed by X-ray diffraction, and valentinite ($Sb_2O_{3(romb.)}$) was the only phase detected. The senarmontite was in the form of large octahedral crystals (10 to 15 mm). The crystals were crushed to 2 to 5 mm in size and washed with HCl and H_2O. Only well-crystallized senarmontite ($Sb_2O_{3(cub.)}$) was detected in the sample by X-ray diffraction, but chemical analysis showed a small amount of As_2O_3 (2.2 wt %).

Valentinite and senarmontite solubility were measured at 80 ± 0.5°C in oxygen-free distilled water. The solids were put in glass flasks placed in a water thermostat and periodically shaken. Solution samples were extracted and immediately filtered through a 1.0-μm paper filter at the temperature of the experiment (80°C). To avoid Sb precipitation, the samples were acidified with HCl. Aqueous antimony concentrations was determined by flame atomic absorption spectrometry with a Varian AA-875 spectrophotometer. Experimental results are listed in Table A1. It can be seen that the solution reached equilibrium with valentinite in less than 4 days. The higher solubility of Valentinite-2 compared with that of Valentinite-1 may reflect a poorer crystallinity of Valentinite-2. For this reason, only the solubility of well crystallized Valentinite-1 was used in the thermodynamic calculations presented in this article. The dissolution of senarmontite was considerably slower than that of valentinite. Steady-state Sb concentrations were not achieved even after 20 d of the experiment (Table A1). Extrapolation of these dissolution-kinetic measurements as a function of time yields a Sb concentration of approximately $(1.1 \pm 0.2) \times 10^{-4}$ mol Sb·(kg H_2O)$^{-1}$ in solution in equilibrium with senarmontite.

APPENDIX 2

Senarmontite Solubility in H_2O at 350°C and Saturated Vapor Pressure

Dissolution experiments were performed with natural senarmontite (see Appendix 1). Solubility was measured at 350 ± 3°C and P_{sat} in oxygen-free distilled water. The experiments were performed in ~20 cm^3 titanium-alloy (VT-8) autoclaves placed vertically in an oven. The solid/solution ratio was ~1:50. The crystals were put in a sample holder located in the upper part of the autoclave to ensure that they were not in contact with the solution at ambient temperature. As temperature increased, the expanded solution came in contact with the Sb_2O_3 crystals. At the end of the run, the autoclave was quenched in cold water to rapidly separate crystals from solution. The solubility was determined by the weight-loss method (Table A2). It was shown by Popova et al. (1975) that equilibrium between senarmontite crystals and solution is achieved within 3 to 4 d at 200°C at solid/solution ratios close to those at in our runs. To ensure that equilibrium was attained in our experiments, the runs lasted 8 to 10 d twice that of the experiments of Popova et al. (1975). Moreover, a recent XAFS spectroscopy study (Pokrovski G., Roux J., Testemale D., and Hazemann J–L., unpublished data) showed that Sb aqueous species attain equilibrium with senarmontite within an hour at temperatures above 300°C and solid/solution ratios of ~1:5.

Table A1. Measured solubility of valentinite and senarmontite in H_2O at 80°C and log $K^0_{(1,\,2)}$ at the 0.95 confidence level.

Solid phase	Time (d)	$m_{Sb} \times 10^4$ (mol·(kg H_2O)$^{-1}$)	log $K^0_{(1,\,2)}$
Valentinite-1	4	2.03	
	7	1.80	
	11	2.26	
	20	2.01	
		2.02 ± 0.3[a]	−3.69 ± 0.06
Valentinite-2	4	2.31	
	7	2.44	
	11	2.33	
	20	2.43	
		2.38 ± 0.12[a]	−3.62 ± 0.02
Senarmontite	4	0.588	
	7	0.808	
	11	0.926	
	20	1.040	
		1.1 ± 0.2[b]	−3.96 ± 0.08

[a] Average value.
[b] Approximated value.

Table A2. Measured senarmontite solubility in H_2O at 350°C and vapor saturation pressure and log $K^0_{(2)}$ at the 0.95 confidence level.

Time (d)	$m_{Sb} \times 10^4$ (mol·(kg H_2O)$^{-1}$)	log $K^0_{(2)}$
8.5	647	
	637	
	623	
9.5	780	
	739	
	756	
	724	
	701 ± 60[a]	−1.15 ± 0.04

[a] Average value.

APPENDIX 3

Measurements of Standard Molal Gibbs Free Energy of Formation of $Sb_2O_{3(cr)}$ by EMF Method with a Zirconia Solid Electrolyte

The standard molal Gibbs free energy for the formation of Sb_2O_3 was determined by the EMF solid state galvanic cell technique with yttria-stabilized zirconia as the solid electrolyte. The measurements were performed at the Institute of Experimental Mineralogy of RAS (Chernogolovka) by E. Osadchii.

EMF measurements of the cell

$$Re, O_2, Sb_{(s)}, Sb_2O_{3(s)} \mid YSZ \mid 'FeO'_{(s)}, Fe_{(s)}, O_2, Re \qquad (A3\text{-}1)$$

were performed for the temperature range from 869.3 to 902.6 K. Experimental details about cell arrangement, furnace, temperature control, etc., can be found elsewhere (Osadchii et al., 1998). Crushed ultrapure Sb (99.999%) and fine-grained Sb_2O_3 (99.99%) were used. The antimony oxide was the same as that used in the solubility runs (Valentinite-1 in Appendix 1). The reference half-cell was prepared from ultra-pure Fe (99.99%) and "FeO" synthesized from appropriate amounts of ultra–pure Fe_2O_3 (99.99) and metallic iron.

Experimental results are shown in Table A3. Measured $E_{exp.}$ values as a function of temperature (Fig. A3) can be expressed by a straight line

$$E = -0.117832 \cdot T - 152.136. \qquad (A3\text{-}2)$$

This relationship corresponds to the assumption of a constant value of ΔC_p for the equilibrium reaction considered.

The oxygen pressure (P_{O_2}, bar) for the reaction

$$2\ Sb_{(s)} + 1.5\ O_{2(g)} = Sb_2O_{3(s)} \qquad (A3\text{-}3)$$

is related to the EMF (E, mV), temperature (T, K) values and the reference oxygen pressures (P'_{O_2}, bar) by the equation

Table A3. The experimental data, EMF ($E_{exp.}$) and temperature (T), and calculated values $\Delta E = E_{exp.} - E$, obtained for the cell (A3-1).

T (K)	$E_{exp.}$ (mV)	ΔE (mV)
869.3	−254.58	−0.01
879.9	−255.80	0.02
884.0	−256.30	0.00
884.9	−256.40	0.00
893.9	−257.50	−0.04
894.5	−257.50	0.04
902.6	−258.50	−0.01

$$\log P_{O_2} = \log P'_{O_2} - 4FE \times 10^{-3}/(RT \times \ln 10), \quad \text{(A3-4)}$$

where R and F are the gas and the Faraday constant, respectively. The reference oxygen pressures (P'_{O_2}, bar) were obtained from the reaction

$$Fe_{(s)} + 0.5\ O_{2(g)} = 'FeO'_{(s)} \quad \text{(A3-5)}$$

and can be expressed (Fredriksson and Rosén, 1984) by the equation

$$\log P'_{O_2} = -0.8839 - 26506/T + 2.2012 \times \log T. \quad \text{(A3-6)}$$

By combining equations A3-2, A3-4, and A3-6, the following relationship is derived:

$$\log P_{O_{2(A3\text{-}3)}} = 1.492 - 23439/T + 2.2012 \times \log T. \quad \text{(A3-7)}$$

At the temperature of valentinite–senarmontite phase transition (879 K), the values of $\Delta G^\circ_{(A3\text{-}3),879} = 1.5\ RT \cdot \ln 10 \cdot \log P_{O_{2(A3\text{-}3)}}$ and is equal to −112.776 kcal·mol^{-1}. The values of standard molal Gibbs free energy for these phases at 25°C and 1 bar were derived by using the values of S°_{298} and the heat capacity equation for senarmontite and valentinite presented above (Table 6):

$$\Delta_f G^\circ_{298,\ Sb_2O_3(senarmontite)} = -151.332 \pm 0.5\ \text{kcal·mol}^{-1},$$

and

$$\Delta_f G^\circ_{298,\ Sb_2O_3(valentinite)} = -149.604 \pm 0.5\ \text{kcal·mol}^{-1}.$$

The uncertainties on these values mainly stem from the extrapolation of $\Delta_f G^\circ$ from 879 to 298.15 K.

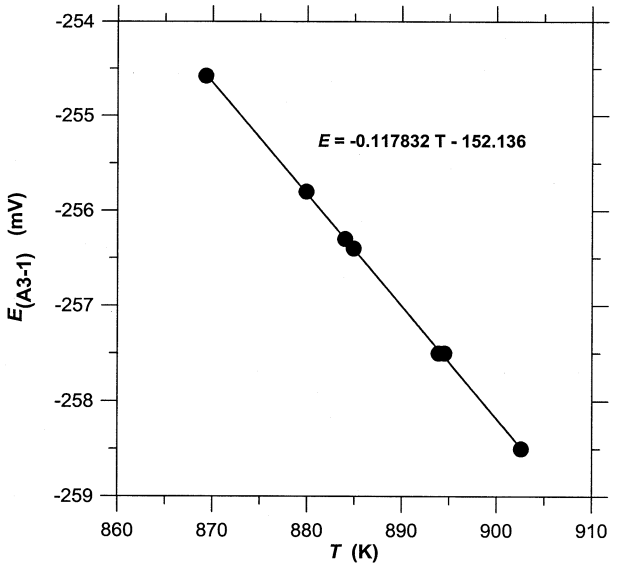

Fig. A3. EMF of the cell (A3-1) as a function of temperature. Symbols are experimental data (Table A3), and the line represents the linear regression of experimental values.

APPENDIX 4

Thermodynamic Properties of $H_2S^\circ_{(aq)}$

As noted by Plyasunov (1991), O'Connell et al. (1996), and Akinfiev (1997), the HKF model for the neutral aqueous species proposed by Shock et al. (1989) is unreliable in the supercritical region, and discrepancies with experiment increase with increasing temperature. For this reason, we used an alternative description for aqueous H_2S based on the equation of state proposed by Akinfiev and Diamond (2003). In brief, the chemical potential ($\mu_2(P, T)$) of a dissolved species at infinite dilution, pressure P (bar) and temperature T (K) is approximated by the empirical equation

$$\mu_2(P,T) = \mu_{2,g}(T) - RT \ln N_w + (1 - \xi)\, RT \ln f_1 + RT\xi \ln\left(\frac{R_V T}{M_1}\rho_1\right) + RT\rho_1 \cdot 2\Delta B, \quad \text{(A4-1)}$$

where $\mu_{2,g}(T)$ stands for the chemical potential of the pure gaseous component at temperature T and standard pressure (1 bar), $R = 1.9872$ cal·mol^{-1}·K^{-1} and $R_V = 83.1441$ cm^3·bar·K^{-1}·mol^{-1} are the gas constants, $N_w = 1000/M_1 \approx 55.51$ mol·kg^{-1}, M_1, f_1, and ρ_1 stand for molar mass (g·mol^{-1}), fugacity (bar), and density (g·cm^{-3}) for the pure solvent (H_2O) at the P-T conditions of interest, respectively; ξ is the so-called scaling factor that is introduced to describe the difference between intrinsic volumes of H_2O and that of the dissolved molecule (Plyasunov et al., 2000), and ΔB characterizes the difference in the short-range interaction energy between solute and solvent molecules. The temperature dependence of ΔB is given by

$$2\Delta B = a + b\left(\frac{10^3}{T}\right)^{0.5}, \quad \text{(A4-2)}$$

where a and b are adjustable parameters of the model. Differentiating Eqn. A4-1 with respect to pressure and temperature results in expressions for the partial molal volume and heat capacity of the dissolved species:

Table A4. Chemical potentials of aqueous $H_2S_{(aq)}$ (in cal·mol^{-1}) at infinite dilution used in this study. P_{sat} is equal to 1 bar at $T < 100°$ and corresponds to H_2O vapor saturation pressure at higher temperature.

T (°C)	P (bars)					
	P_{sat}	250	500	1000	2000	3000
0	−6131	−5918	−5711	−5314	−4575	−3891
25	−6767	−6563	−6364	−5979	−5254	−4576
50	−7509	−7307	−7109	−6726	−6004	−5327
75	−8337	−8133	−7933	−7547	−6820	−6139
100	−9241	−9031	−8827	−8434	−7696	−7007
125	−10211	−9995	−9784	−9380	−8628	−7927
150	−11243	−11018	−10798	−10381	−9610	−8896
175	−12332	−12098	−11867	−11433	−10639	−9910
200	−13475	−13230	−12985	−12531	−11711	−10965
225	−14671	−14414	−14152	−13673	−12823	−12059
250	−15919	−15650	−15365	−14856	−13972	−13188
275	−17221	−16940	−16623	−16077	−15156	−14350
300	−18583	−18289	−17927	−17336	−16372	−15542
325	−20021	−19711	−19279	−18629	−17617	−16764
350	−21581	−21239	−20682	−19956	−18891	−18012
375		−23051	−22143	−21314	−20190	−19284
400		−25867	−23675	−22703	−21512	−20580
425		−27308	−25295	−24119	−22856	−21897
450		−28690	−26984	−25560	−24220	−23234
475		−30071	−28630	−27021	−25602	−24589
500		−31460	−30160	−28497	−27000	−25961
525		−32861	−31619	−29979	−28412	−27349
550		−34274	−33050	−31460	−29836	−28751
575		−35701	−34475	−32936	−31271	−30166
600		−37140	−35901	−34406	−32716	−31594

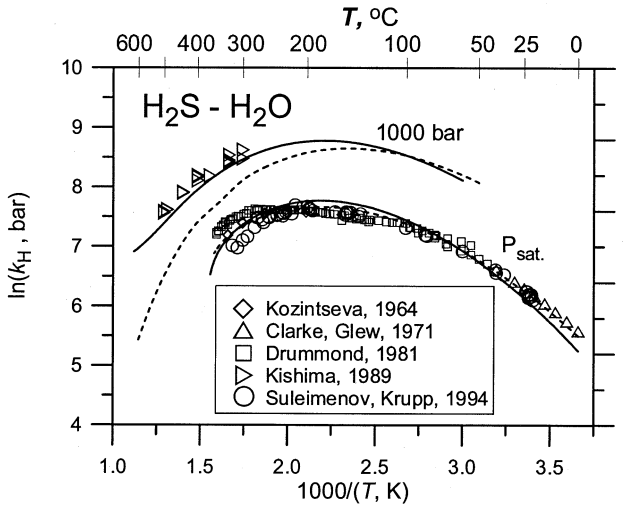

Fig. A4-1. Values of the Henry constant for H_2S at saturated vapor pressure ($P_{sat.}$) and 1000 bar total pressure plotted against reciprocal temperature. Symbols correspond to the experimental data, the solid curves are the model predictions. The dashed curves indicate predictions of the HKF model with data from the SUPCRT92 package (Johnson et al., 1992).

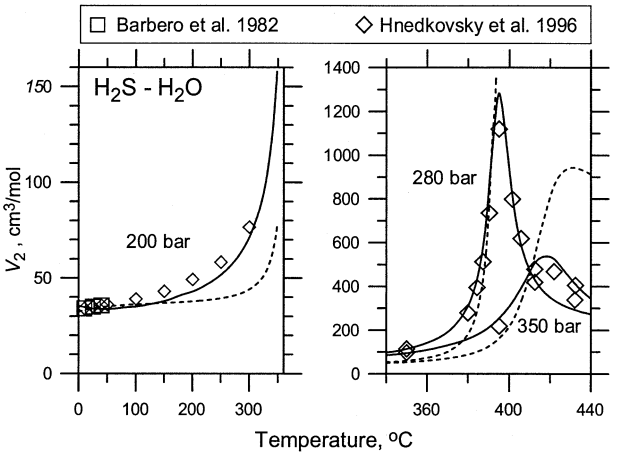

Fig. A4-3. Apparent molar volumes of aqueous H_2S at 350 bar as a function of temperature. Symbols correspond to experimental data for an H_2S molality of approximately 0.248, from Hnědkovsky et al. (1996), and the solid curve is the model prediction for infinite dilution. The dashed curve indicates the prediction of the HKF model with data from the SUPCRT92 package (Johnson et al., 1992).

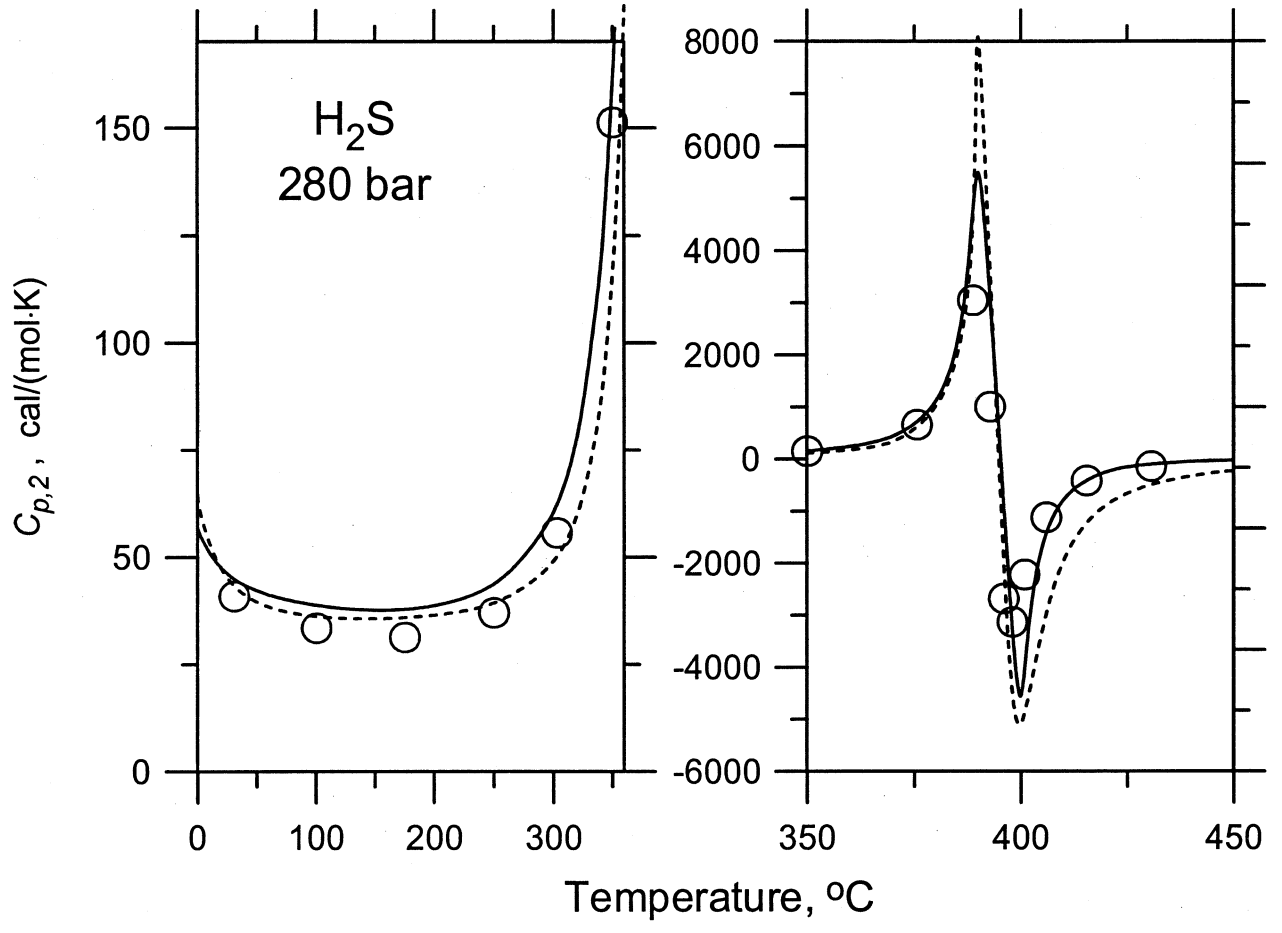

Fig. A4-2. Apparent molar heat capacity of aqueous H_2S as a function of temperature at 280 bar. Symbols correspond to the experimental data for an H_2S molality of approximately 0.372 (Hnědkovsky and Wood, 1997), and the solid curve is the model prediction for infinite dilution. The dashed curve indicates prediction of the HKF model with data from the SUPCRT92 package (Johnson et al., 1992).

$$V_2 = V_1(1-\xi) + R_V T\frac{1}{\rho_1}\frac{\partial \rho_1}{\partial P} + R_V\frac{\partial}{\partial P}(T\rho_1 \times 2\Delta B) \quad \text{(A4-3)}$$

$$C_{p2} = C_{p2,g} + (1-\xi)(C_{p1} - C_{p1,g}) - R\left(\xi + 2\xi\frac{1}{\rho_1}\frac{\partial \rho_1}{\partial T} - \xi\frac{T}{(\rho_1)^2} + \xi T\frac{\partial^2 \rho_1}{\partial T^2}\right) - RT\frac{\partial^2}{\partial T^2}(T\rho_1 2\Delta B) \quad \text{(A4-4)}$$

Here, as before, index g stands for ideal gaseous component at the T of interest and standard pressure, index 1 denotes pure H_2O, and 2 denotes the solvent.

Assuming $V_2 = 34.8$ cm^3·mol^{-1} (Hnědkovsky et al., 1996), and taking into account the complete set of experimental data for the Henry constant of H_2S covering both subcritical (Kozintseva, 1964; Clarke and Glew, 1971; Drummond, 1981; Namiot, 1991; Suleimenov and Krupp, 1994) and supercritical (Kishima, 1989) regions of H_2O, a set of data for the following empirical parameters was retrieved: $\xi = -0.202$, $a = -11.4803$ cm^3·g^{-1}, and $b = 12.7158$ cm^3·K$^{0.5}$·g^{-1} (Akinfiev and Diamond, 2003). The fit quality is illustrated in Figs. A4-1 to A4-3. It can be seen that there is good agreement between the experimental data and corresponding calculated values. Predictions of the HKF model with data from the SUPCRT92 package (Johnson et al., 1992) are given as dashed lines for comparison. For the convenience of readers, calculated values of chemical potentials of aqueous $H_2S°_{(aq)}$ at infinite dilution used in this study are given in Table A4.

APPENDIX 5

Senarmontite Solubility in H_2O-N_2 Mixed Fluids at 400°C and 500 bars

Dissolution experiments were performed by using natural and synthetic senarmontite occurring in the form of large octahedral crystals (2 to 8 mm). The natural senarmontite was from Algeria (see Appendix 1); synthetic crystals were prepared in the Institute of Crystallography of the Russian Academy of Sciences by use of the fluoride method (Popolitov, 1989). Only senarmontite was detected by X-ray diffraction of these crystals. Senarmontite solubility was measured at 400 ± 3°C and a pressure of 500 ± 50 bars. The experiments were carried out in the Ti autoclaves described in Appendix 2. Fluids of different compositions were prepared by introducing mass ratios of H_2O and liquid N_2 into the autoclave. The duration of runs was 4 to 6 d. After quenching at the end of a run, the mole fraction of N_2 was determined by weighing on an Acculab LT-3200 balance, and the concentration of Sb was measured by the weight-loss method with an Ohaus analytical balance. The measured values of equilibrium Sb concentration (mol Sb per kg H_2O) as a function of mole fraction of N_2; and calculated values of pressure, fluid dielectric permitivity, and dielectric correction factor are presented in Table A5. For H_2O-N_2 mixed fluids, the values of pressure and dielectric permitivity were calculated by the Redlich-Kwong equation and the modified Kirkwood equation, respectively. Details of these calculations are given by Akinfiev and Zotov (1999).

Table A5. Senarmontite solubility in the mixed H_2O-N_2 fluid at 400°C and 500 ± 50 bar.

P (bars)	X_{N2} (mole fraction)	m_{Sb} (mol·(kg H_2O)$^{-1}$)	log m_{Sb} −1.5 log α_{H_2O}[a]	Dielectric permittivity (ε)	Dielectric correction factor
500	0	0.072 ± 0.005	−1.14	12.263	0
490	0.05	0.063	−1.17	7.575	1.67
490	0.05	0.061	−1.18	7.575	1.67
495	0.05	0.058	−1.20	7.575	1.68
454	0.10	0.052	−1.22	4.135	5.05
454	0.10	0.045	−1.28	4.135	5.05
452	0.10	0.049	−1.24	4.135	5.11
480	0.18	0.025	−1.16	3.124	7.69
515	0.31	0.014	−1.61	2.435	10.73
535	0.33	0.01	−1.74	2.415	10.89

[a] Activity of H_2O is assumed to be equal to its mole fraction.

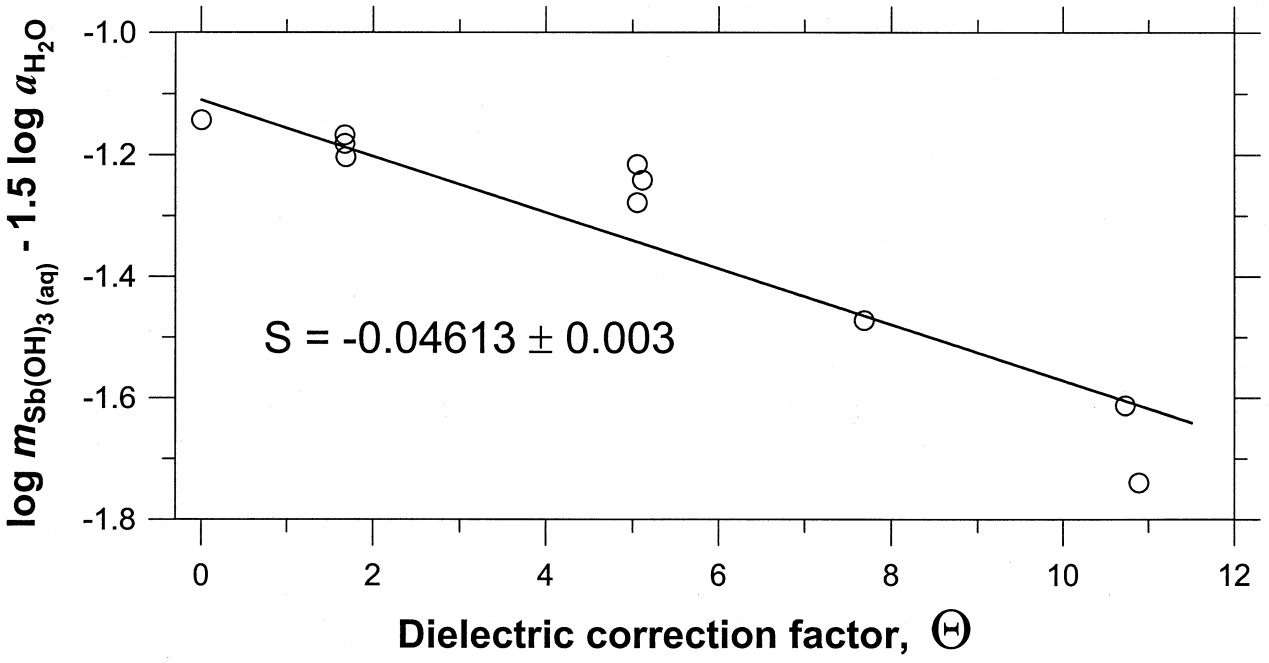

Fig. A5. Logarithm of constants for reaction 2 as a function of the dielectric correction factor (Θ; see text) in mixed H_2O-N_2 fluids at 400°C and 500 ± 50 bars. The symbols denote experimental data (Table A5); and the curve represents a linear regression of these values. The slope S of the linear regression corresponds to the value for the Born parameter ($-\omega$) of $Sb(OH)_{3(aq)}$.